Exploring the requirements and regulation of anillin as a target of the chromatin pathway in mammalian cells

Noha Skaik

A

Thesis

In the Department

Of

Biology

Presented in Partial Fulfillment of the Requirements

For the Degree of

Master of Science (Biology) at

Concordia University

Montreal, Quebec, Canada

August 2020

CONCORDIA UNIVERSITY

School of Graduate Studies

This is to certify that the thesis prepared

By: Noha Skaik

Entitled: Exploring the requirements and regulation of anillin as a target of the chromatin pathway in mammalian cells

and submitted in partial fulfillment of the requirements for the degree of

Master of Science (Biology)

complies with the regulations of the University and meets the accepted standards with respect to originality and quality.

Signed by the final Examining Committee:

_____ Chair
Dr. William Zerges

_____ External Examiner
Dr. Vladimir Titorenko

_____ Examiner
Dr. Malcolm Whiteway

_____ Examiner
Dr. William Zerges

_____Thesis Supervisor(s)
Dr. Alisa Piekny

Approved by _____
Dr. Robert Weladji, Graduate Program Director

_____

Pascale Sicotte, Dean of Faculty of Arts and Science

Thursday, August 27th , 2020_____

Abstract

Exploring the requirements and regulation of anillin as a target of the chromatin pathway in mammalian cells

Noha Skaik

This thesis explores the requirement of anillin, a cytokinesis regulator, in different human cell types and the mechanism that regulates anillin function. Cytokinesis is the process that physically separates a cell into two daughter cells. It takes place during mitotic exit to complete the cell cycle. Cytokinesis is spatiotemporally controlled to ensure that each daughter cell inherits the proper distribution of genomic and cytoplasmic content. Dysregulation of cytokinesis is correlated with diseases such as cancer. In metazoan cells, cytokinesis relies on the assembly and ingression of an actomyosin ring that pinches in the overlying membrane. Anillin is a scaffold protein with multiple binding partners that crosslinks the actomyosin ring to the membrane. Multiple conserved mechanisms regulate cytokinesis, and some mechanisms may be favored over others depending on the cell type. Our lab recently discovered a chromatin-based pathway that regulates ring assembly and position through anillin. We propose that this pathway is more strongly required in cancer cells with high aneuploidy, which typically arises during cancer progression. In support of this model, we found that anillin depletion causes a higher incidence of cytokinesis failure in cancer cells with higher aneuploidy. Using CRISPR-Cas9 to endogenously tag anillin, we define the thresholds of anillin required to support cytokinesis in different cell types. We also explored the mechanism regulating anillin function, and found that the chromatin pathway controls phospholipid binding required for the cortical recruitment of anillin. My findings revealed how the chromatin pathway controls the molecular function of anillin for cytokinesis.

Acknowledgments

I would like to thank my supervisor, Dr. Alisa Piekny. Thank you for believing in me and providing me with this opportunity. It was such an honor to be your student.

I would also like to thank my committee members, Dr. Malcolm Whiteway and Dr. William Zerges. Thank you for your time and support throughout the project.

I would also like to thank Dr. Chris law, The Centre for Microscopy and Cellular Imaging (CMCI). Thank you for your constant help and guidance throughout my imaging sessions.

Lastly, I would like to thank the Piekny lab members. Nhat, thank you for teaching me the basics in the lab. Imge, Mathieu, Kevin, Su pin, Nhat, Victoria, Mathew, Joe, Dilan, Karina and Stephanie, thank you for your moral support and the pep talks. It was a pleasure to work with all of you!

Dedications

Praise is to Allah by whose grace good deeds are completed.

Mama and Baba, this is for you.

To mama, it has been 5 years since you passed away... Yet, your strength has always been my motivation. We miss you so much. May the Almighty grant you paradise.

To Baba, thank you for always believing in me before I believe in myself. Your constant scarification for us is indispensable.

Contribution of authors

Figure 2. The pathway was drawn by Dr. Daniel Beaudet.

Figure 7. Brandon Jaunky and Kevin Larocque performed the immunofluorescence, and Dr. Su Pin Koh performed the western blots.

Figure 8. Dr. Su Pin Koh and Kevin Larocque performed the $CoCl_2$ treatment, RNAi and immunofluorescence.

Figure 9. Mathieu Husser performed the endogenous tagging of anillin using CRISPR-Cas9, and I performed the live imaging.

Figure 13. Dr. Daniel Beaudet used PyMOL software to draw the ribbon structure of anillin.

Figure 14. The pull-down experiments were performed by Dr. Daniel Beaudet and Nhat Pham. I performed the transfections and western blots.

Figure 15. I made the mutant using PCR-based site directed mutagenesis and Dr. Daniel Beaudet performed the live imaging.

Figure 17. The model was drawn by Dr. Daniel Beaudet.

Table of Contents

List of Figures

List of abbreviations

AHD	Anillin homology domain
C-terminus	Carboxyl-terminus
C2	Protein kinase C conserved lipid binding region 2
Cdk1	Cyclin-dependent kinase 1
CPC	Chromosomal passenger complex
Cyk-4	Cytokinesis defect 4
DH	Db1 homology domain
Ect2	Epithelial cell transforming 2
F-actin	Filamentous-actin
GDP	Guanosine diphosphate
GEF	Guanine nucleotide exchange factor
GTP	Guanosine triphosphate
mDia	Mammalian diaphanous
MKLP1	Mitotic kinesin like protein 1
MP-GAP	M-phase GTPase activating protein
N-terminus	NH_2-terminus
NLS	Nuclear localization signal
PH	Pleckstrin homology domain
PI_3P	Phosphatidylinositol 3-phosphate
$PI_{4,5}P_2$	Phosphatidylinositol 4,5-bisphosphate
Plk1	Polo-like kinase 1
PP1-Sds22	Protein phosphatase 1and its regulatory subunit Sds22
PRC1	Protein regulator of cytokinesis 1
Ran	Ras-related nuclear protein GTPase
RanGAP	Ran GTPase activating protein
RBD	RhoA binding domain
RCC1	Regulator of chromosome condensation 1
RhoA	Ras homology family member A
TPX2	Targeting Protein for Xklp2

Chapter 1. Introduction

1.1 Cytokinesis Overview

The assembly and ingression of the contractile ring is the fundamental driving force of cytokinesis (Glotzer, 2017; Pollard, 2017; Figure 1; Figure 2). In animal cells, the first visible component of the contractile ring is the enrichment of active RhoA in the equatorial plane during anaphase. This pool of active RhoA is generated by the guanine nucleotide exchange factor (GEF) Ect2, while RhoA is downregulated at other regions of the cortex by MP-GAP (Figure 2). Active RhoA binds to multiple effectors including formin and Rho kinase for actomyosin filament assembly that leads to force generation through constriction (Basant & Glotzer, 2018; Piekny et al., 2005). RhoA also recruits anillin to the equatorial plane (Piekny & Glotzer, 2008; Figure 1). Anillin is a highly conserved contractile ring protein with binding sites for actin, myosin, RhoA, phospholipids, microtubules and septins, among others, and crosslinks actomyosin to the overlying plasma membrane for ring positioning (Green et al., 2012; Piekny & Glotzer, 2008; Piekny & Maddox, 2010). Anillin stabilizes RhoA at the equatorial cortex (Beaudet et al., 2020; Budnar et al., 2019; Figure 2). It also regulates the maturation of the contractile ring to the midbody ring, which requires the shedding of membrane and ring components to form a stable midbody that is required for abscission (El Amine et al., 2013; Kechad et al., 2012).

Regulators that mediate ring assembly and constriction are essential to support cytokinesis. Specifically, the loss of key regulators, including Ect2, RhoA, formin or Rho kinase causes early cytokinesis phenotypes in metazoan cells including those in *C. elegans*, Drosophila, *Xenopus*, and mammals (Piekny et al., 2005; Piekny & Glotzer, 2008; Reyes et al., 2014; Yüce et al., 2005). In these cells, the ring fails to form, or forms but fails to ingress. In anillin-depleted cells, the ring either ingresses more symmetrically vs. asymmetrically (*e.g.* early *C. elegans* embryo), or its position is not stable and the ring oscillates around the cell (Drosophila S2 cells, or HeLa cells) (Maddox et al., 2007; Piekny & Glotzer, 2008; Straight et al., 2005). However, anillin depletion also causes later cytokinesis phenotypes consistent with its role in midbody ring transition (Kechad et al., 2012), likely reflecting its different threshold requirements for these different processes.

A

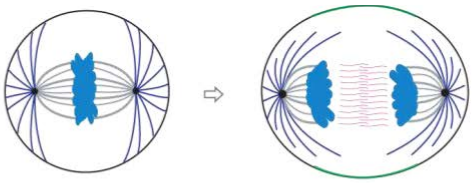

Establishment of division plane

B

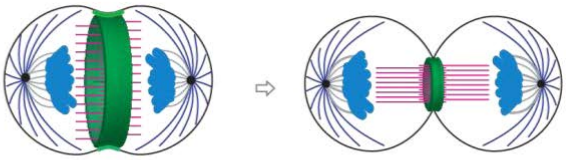

Furrow ingression

C

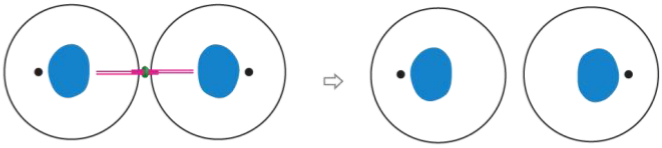

Abscission

Figure 1. An overview of cytokinesis. Cytokinesis occurs at the end of mitosis to physically separate the daughter cells. A. In anaphase onset, signals establish the division plane, where distribution of cytokinesis regulators take place. Specifically, the central spindle microtubules start to bundle (pink) between segregated chromosomes (blue) in addition to the localization of other core cytokinesis regulators. One of the regulators is anillin, which gets recruited to the equatorial cortex (green). B. The assembly and ingression of an actomyosin ring leads to furrow ingression of the overlying membrane to pinch in the daughter cells (green). C. The contractile ring transitions into a midbody ring and initiates abscission that leads to the physical separation of the daughter cells.

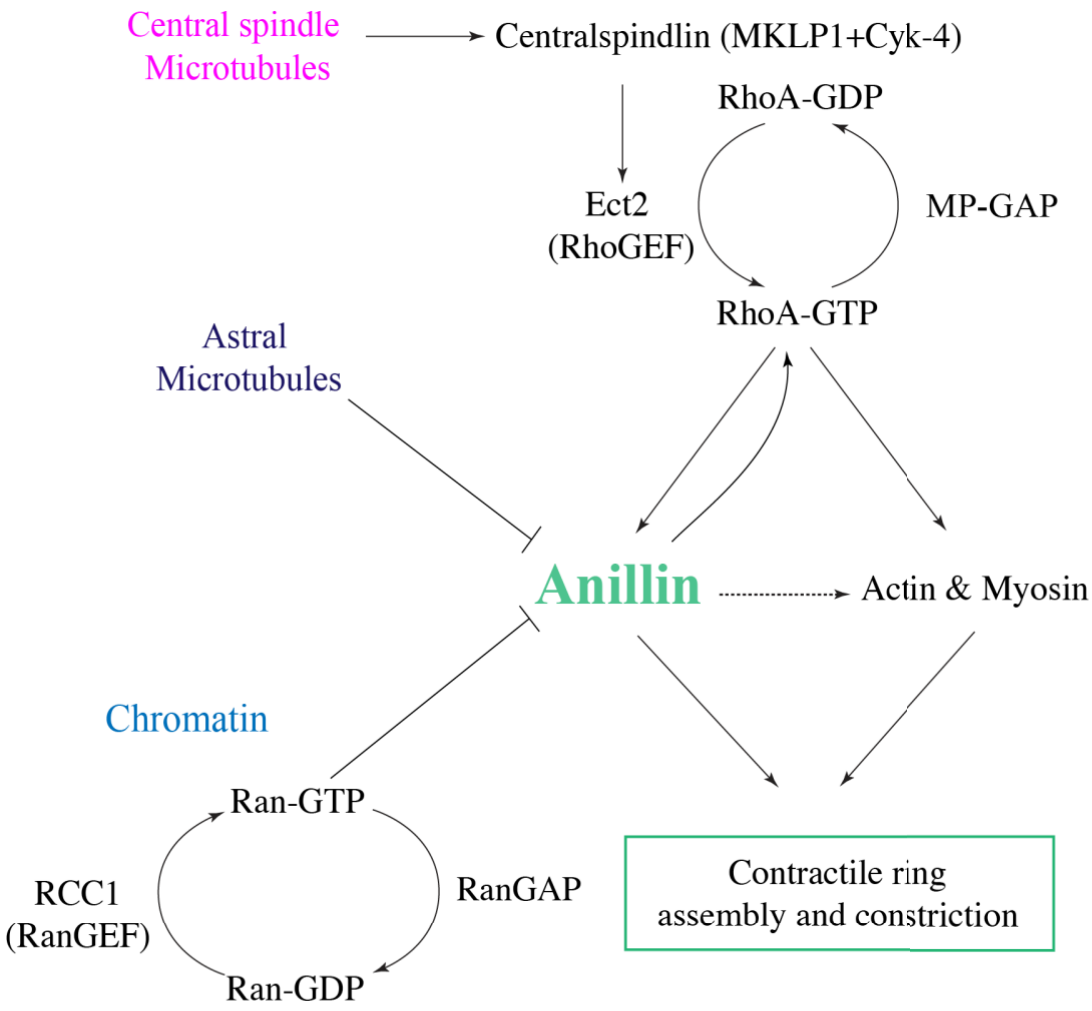
Central spindle
Microtubules
Centralspindlin (MKLP1+Cyk-4)
RhoA-GDP
Ect2
(RhoGEF)
MP-GAP
RhoA-GTP
Astral
Microtubules
Anillin
Actin & Myosin
Chromatin
Ran-GTP
RCC1
(RanGEF)
RanGAP
Ran-GDP
Contractile ring
assembly and constriction

Figure 2. Cytokinesis regulators mediate ring assembly and ingression. Spindle dependent and -independent pathways regulate cytokinesis. Cytokinesis is initiated through activation of the master regulator RhoA-GTP. Specifically, centralspindlin activates Ect2 (RhoA GEF). This in turn activates RhoA-GTP, which activates anillin, actin, and myosin to initiate contractile ring assembly and constriction. Anillin stabilizes active RhoA at the equatorial cortex. Concurrently, astral microtubules and chromatin pathways regulate cytokinesis through affecting the position of anillin.

Multiple spindle dependent and -independent pathways work together to regulate contractile ring assembly or positioning (Figure 2). In animal cells, the anaphase spindle has associated signals that controls the position and assembly of the actomyosin ring (Fededa & Gerlich, 2012; Green et al., 2012; Pollard & O′Shaughnessy, 2019). Signals associated with other locations and organelles including chromatin, centrosomes and kinetochores also influence ring positioning or ingression kinetics (Beaudet et al., 2017; Kiyomitsu & Cheeseman, 2013; Mangal et al., 2018; Rodrigues et al., 2015; Zanin et al., 2013). The requirement of a pathway likely varies among cell types depending on characteristics such as cell size, symmetry, ploidy and fate. However, some of the spindle-independent pathways are newly discovered and are not well-understood, and few studies have explored the regulation of cytokinesis *in vivo*.

1.2 Spindle-dependent pathways

The division plane is spatially defined by the anaphase spindle, which is composed of the central spindle and astral microtubules. The central spindle forms in anaphase, and consists of antiparallel bundled microtubules that arise between the segregating chromosomes (Mishima et al., 2002, 2004). Centrosome-derived astral microtubules emanate toward the cell poles. Proteins associated with the central spindle and/or astral microtubules control the breadth of active RhoA in the equatorial cortex, which is initially broad, but then becomes narrower as the ring ingresses (Basant et al., 2015; D′Avino et al., 2015; Fededa & Gerlich, 2012; Yüce et al., 2005; Zanin et al., 2013).

The central spindle is associated with the generation of active RhoA (Figure 3). Centralspindlin is a heterotetrametric complex that is composed of dimers of the kinesin motor MKLP1 and Cyk4/MgcRacGAP, and is essential for central spindle assembly in metazoan cells (Glotzer, 2009; Mishima et al., 2002, 2004; Pavicic-Kaltenbrunner et al., 2007). In addition, Cyk4 forms an anaphase-dependent complex with Ect2 that is required to generate active RhoA (Basant & Glotzer, 2018; Kotýnková et al., 2016; Lekomtsev et al., 2012; Yüce et al., 2005). This is accomplished by the interplay between Cdk1, Polo-like kinase 1 (Plk1), and Aurora B kinase (Basant et al., 2015; Hara et al., 2006; Niiya et al., 2006; Petronczki et al., 2007; Wolfe et al., 2009). The inactivation of Cdk1 at mitotic exit corresponds with the dephosphorylation of Ect2, presumably to relieve its autoinhibition of the C-terminal DH domain which is required for nucleotide exchange (Fededa & Gerlich, 2012; Hara et al., 2006; Yüce et al., 2005). Concurrently,

phosphorylation of Cyk4 by Plk1 is required for Ect2-binding and to facilitate GEF activity, although how Cyk4-binding modulates GEF activity is not known (Adriaans et al., 2019; Niiya et al., 2006; Petronczki et al., 2007; Wolfe et al., 2009). The depletion or loss-of-function alleles of Cyk4 and Ect2 have the same phenotype, where active RhoA is no longer generated and the contractile ring fails to form (Kamijo et al., 2006; Nishimura and Yonemura, 2006; Yüce et al., 2005; Zhao & Fang, 2005). Until recently, the prevailing model was that Cyk4-binding recruits Ect2 to the central spindle, where it helps spatiotemporally activate Ect2 to generate active RhoA at the overlying membrane. However, studies showed that the membrane-binding domains of Ect2 and Cyk4 are essential for GEF activity, while the central spindle itself is dispensable (*e.g.* via depletion of core regulators of central spindle assembly such as PRC1) (Kotýnková et al., 2016; Mollinari et al., 2005; Yüce et al., 2005). It is still not known how or where the Cyk4-Ect2 complex forms, and how it can generate RhoA in such a well-defined zone. Ect2 localizes to the central spindle and equatorial cortex in mammalian cells, but is primarily at the anterior cortex in one-cell *C. elegans* embryos, while neither Cyk4 or MKLP1 are detectable at the cortex in most cells (Basant & Glotzer, 2018; Yüce et al., 2005). Recently, Cyk4 was shown to localize to the plus-ends of bundled astral and/or central spindle microtubules where it colocalizes with cortical Ect2 in Drosophila S2 cells (Verma and Maarsca, 2020). While this does not explain how the complex transitions from microtubules to the cortex, having them in close proximity could facilitate their movement via other proteins.

Aurora B kinase also influences ring assembly. Aurora B kinase is part of the chromosomal passenger complex (CPC) which transitions from the kinetochores to the central spindle, and helps mediate central spindle assembly (Basant et al., 2015; Basant & Glotzer, 2018; Fededa & Gerlich, 2012; Guse et al., 2005). During anaphase, Aurora B kinase phosphorylates MKLP1, which is required for generating a stable midbody (Douglas et al., 2010; Guse et al., 2005; Figure 3). Clustering of the centralspindlin complex is inhibited by the binding of 14-3-3 protein to MKLP1, preventing its localization to the central spindle. Additional studies found that Aurora B kinase phosphorylation to MKLP1 antagonizes 14-3-3 binding, resulting in the clustering and localization of centralspindlin to the central spindle (Basant et al., 2015; Douglas et al., 2010). Although less clear, this may also occur at the overlying cortex. A recent study showed that the Aurora B kinase/14-3-3 regulation of centralspindlin could influence the generation of active RhoA at the equatorial plane for furrowing. In one-cell *C. elegans* embryos or cultured human cells treated with

PRC1 RNAi to disrupt central spindle assembly, contractile rings still form and ingress, and there is an increase in the cortical enrichment of Aurora B kinase which could generate active RhoA through regulating Cyk4-Ect2 complexes (Adriaans et al., 2019). A model was proposed where a membrane-specific pool of Plk1-regulated Cyk4-Ect2 complexes facilitate ring assembly, while the central spindle pool acts as a sink (Adriaans et al., 2019; Figure 3).

Astral microtubules negatively regulate cytokinesis by controlling the breadth of RhoA localization (Basant & Glotzer, 2018; Green et al., 2012; Werner et al., 2007). Although the mechanism is unknown, astral microtubules promote the removal of contractile proteins from the polar cortex including RhoA, anillin, and myosin (van Oostende Triplet et al., 2014; Zanin et al., 2013). Experiments utilizing RNAi or microtubule-targeting drugs to depolymerize microtubules caused an increase in the breadth of contractile proteins, while increasing the length or stability of astral microtubules caused a more narrow distribution (van Oostende Triplet et al., 2014; Zanin et al., 2013). One mechanism is that astral microtubules control the distribution of contractile proteins through anillin, which directly binds to microtubules (Tse et al., 2011; van Oostende Triplet et al., 2014). Depleting anillin in cells with increased length or stability of astral microtubules restores the normal breadth of contractile proteins (van Oostende Triplet et al., 2014). In addition, there is an increase in anillin localization to microtubules when the levels of active RhoA are decreased, suggesting that there is a negative correlation between RhoA vs. microtubule-binding (van Oostende Triplet et al., 2014). However, the mechanism by which anillin facilitates the clearance of contractile proteins from the poles is unknown. A recent study showed that the activation of Aurora A kinase at astral microtubules by TPXL-1 (*C. elegans* TPX2), which is a microtubule associated protein required for mitotic spindle assembly, facilitates the clearance of anillin and myosin from the cell poles in the early C. *elegans* embryo (Mangal et al., 2018). The relative contribution of astral microtubules vs. central spindle to defining the equatorial plane varies depending on cell-type and organism (Glotzer, 2017; Ozugergin & Piekny, 2020; Tse et al., 2011). One hypothesis is that astral microtubules could be more predominant than the central spindle in cells where the central spindle is smaller and located further from the cortex, and could explain differences in requirements for the underlying mechanisms.

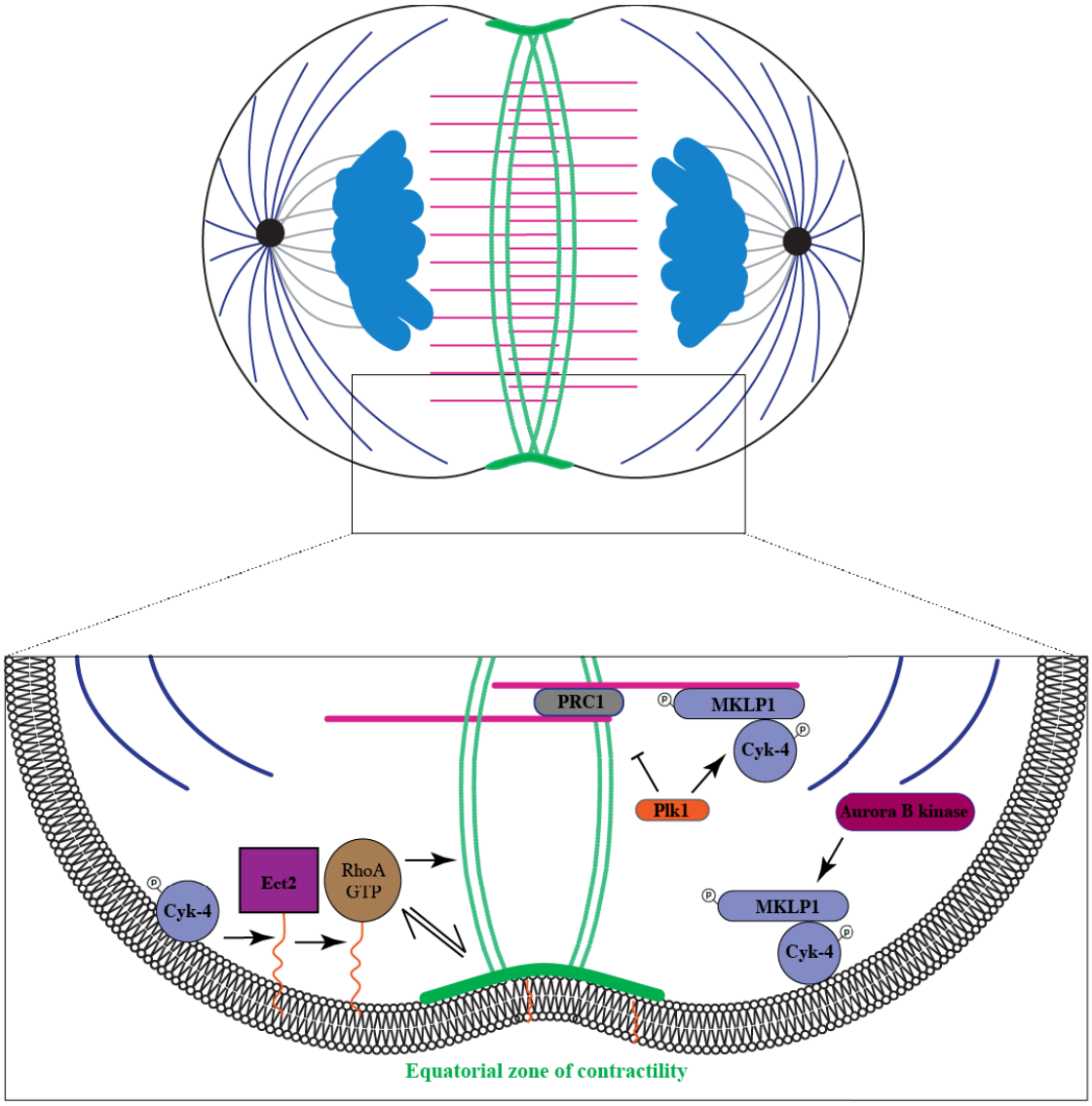
PRC1
MKLP1
Cyk-4
Plk1
Aurora B kinase
Ect2
RhoA
GTP
Cyk-4
MKLP1
Cyk-4
Equatorial zone of contractility

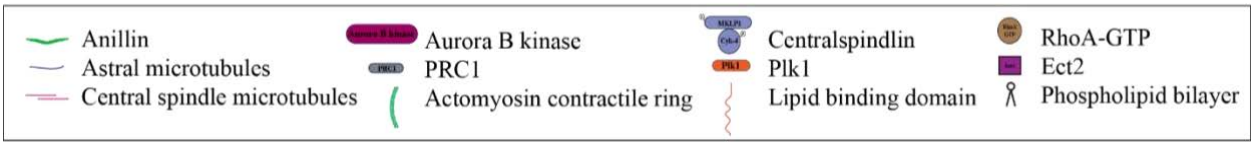
Anillin
Astral microtubules
Central spindle microtubules
Aurora B kinase
PRC1
Actomyosin contractile ring
Centralspindlin
Plk1
Lipid binding domain
RhoA-GTP
Ect2
Phospholipid bilayer

Figure 3. The role of the central spindle in initiating cytokinesis. The bundling and assembly of the central spindle requires PRC1 and centralspindlin (MKLP1+Cyk-4). MKLP1 and Cyk-4 get phosphorylated by Aurora B kinase and Plk1, respectively. Centralspindlin is required to create an active zone of RhoA at the region of contractility. Specifically, phosphorylated Cyk-4 activates Ect2 (RhoA GEF) which generates RhoA-GTP. Active RhoA initiates actomyosin assembly and contractility. A model was recently proposed where Plk1 inhibition to PRC1 and Aurora B kinase work redundantly to create a pool of centralspindlin at the cortex to initiate cytokinesis (Adriaans et al., 2019).

1.3 Spindle-independent pathways

Microtubule-independent mechanisms have also been shown to spatially regulate cytokinesis. Signals arising from different subcellular locations affect the localization of contractile proteins. For example, the cortical protein M phase GTPase activating protein (MP-GAP), which is a GAP that promotes hydrolysis of GTP to inactivate RhoA, works with astral microtubules to globally inactivate and restrict active RhoA to the equatorial cortex in mammalian cells and the one-cell C. *elegans* embryo (Zanin et al., 2013). In addition, active Rac may be reduced at the equatorial cortex to facilitate the formation of long branched F-actin via RhoA. Although this is heavily debated in the field, Cyk4 has GAP activity toward several Rho-family GTPases *in vitro.* While it is required for RhoA activation via Ect2-binding in cells, its GAP domain could downregulate Rho GTPases in the equatorial plane. However, it is not clear that this occurs *in vivo*. RNAi of *ced-10* (C. *elegans* Rac) or *arp-2/3* (regulates branched F-actin assembly) partially suppresses *cyk-4* RNAi to permit some furrowing (Canman et al., 2008). However, this could be interpreted in two very different ways. One interpretation is that CYK-4 is required to downregulate CED-10, and loss of CYK-4 causes hyperactive CED-10, which is suppressed when reduced. Another interpretation is that CED-10 is required to control rigidity of the polar cortex, and its reduction softens the cortex to permit furrowing when the contractile ring is improperly formed (Canman et al., 2008). Signals also come from other subcellular locations. A kinetochore-derived pathway was recently shown to induce relaxation of the mitotic polar cortices in cultured mammalian and Drosophila cells. This is accomplished through a kinetochore-tethered PP1 phosphatase-Sds22 complex which dephosphorylates the ezrin/radixin/moesin (ERM) proteins and reduces F-actin crosslinking for relaxation of the polar cortex (Rodrigues et al., 2015). In addition, several studies have shown a correlation between the chromatin position and spatial distribution of contractile proteins in mammalian cells, suggesting the presence of cues emitted from chromatin to regulate cytokinesis (Beaudet et al., 2017, 2020; Kiyomitsu & Cheeseman, 2013; Rodrigues et al., 2015).

1.4 The chromatin pathway

A gradient of active Ran is a radar that informs the cell about chromatin position during mitosis. Although Ran is best known for its role in nucleocytoplasmic transport, it has a well-described function for regulating spindle assembly and kinetochore attachment during metaphase, and more recently we uncovered a role for Ran during cytokinesis. The Ran GEF (RCC1) is

tethered to histones of chromatin where it generates Ran-GTP, while Ran-GAP is enriched in the cytosol to form inactive Ran-GDP at distances away from chromatin (Clarke & Zhang, 2008; Xu & Massagué, 2004). Ran-GTP binds to and removes importin alpha/beta heterodimers from the nuclear localization signal (NLS) of proteins (Clarke & Zhang, 2008; Kalab & Heald, 2008; Soniat & Chook, 2015). During metaphase, Ran-GTP dissociates importins from spindle assembly factors to initiate the formation of a bipolar spindle around chromatin (Forbes et al., 2015; Kalab & Heald, 2008). The model for how this works is that proteins required for spindle assembly are inactive when bound to importins, but when importins are removed, they are able to form active complexes to mediate spindle assembly (Ozugergin and Piekny, 2020). This ensures that a bipolar spindle builds around the chromosomes, and can modulate kinetochore attachments.

During meiosis, chromatin position controls polar body formation to extrude the excess chromosomes. Proteins that form an actin cap, a structure that acts as a precursor to polar body extrusion, accumulate at precise distances away from chromatin and Ran-GTP. Experiments showed that the location of polar body formation changed in response to DNA beads of different sizes (Deng et al., 2007). Thus, Ran-GTP and the inverse gradient of importins were proposed to function as a molecular ruler where optimal concentrations facilitate cortical polarization, but inhibit it at other concentrations (Deng et al., 2007).

During cytokinesis, the Ran pathway regulates cortical polarity via a model that is reminiscent of its control of polar body formation vs. spindle assembly. Our lab and others found that chromatin position inversely correlates with the localization of contractile proteins during cytokinesis (Kiyomitsu & Cheeseman, 2013; Beaudet et al., 2017; Figure 4). In addition, in cells lacking polymerized microtubules and stimulated to exit mitosis, anillin and myosin localized away from chromatin but not when RCC1 (RanGEF) activity was reduced (Kiyomitsu & Cheeseman, 2013). In cells with intact spindles, reducing RCC1 function during cytokinesis caused the ectopic localization of contractile proteins and failed ingression, while the membrane-localization of exogenous active Ran caused proteins to move away from the furrow and displacement of the ring (Beaudet et al., 2017). This data supports a role for the Ran pathway in spatial regulation of the contractile ring for cytokinesis. Our lab also found that anillin is a direct target of this pathway (Figure 4). Anillin has a conserved binding site for importins in its C-terminus, and importin-binding is required to facilitate its cortical localization and function for cytokinesis (Beaudet et al., 2017; Beaudet et al., 2020; Figure 4).

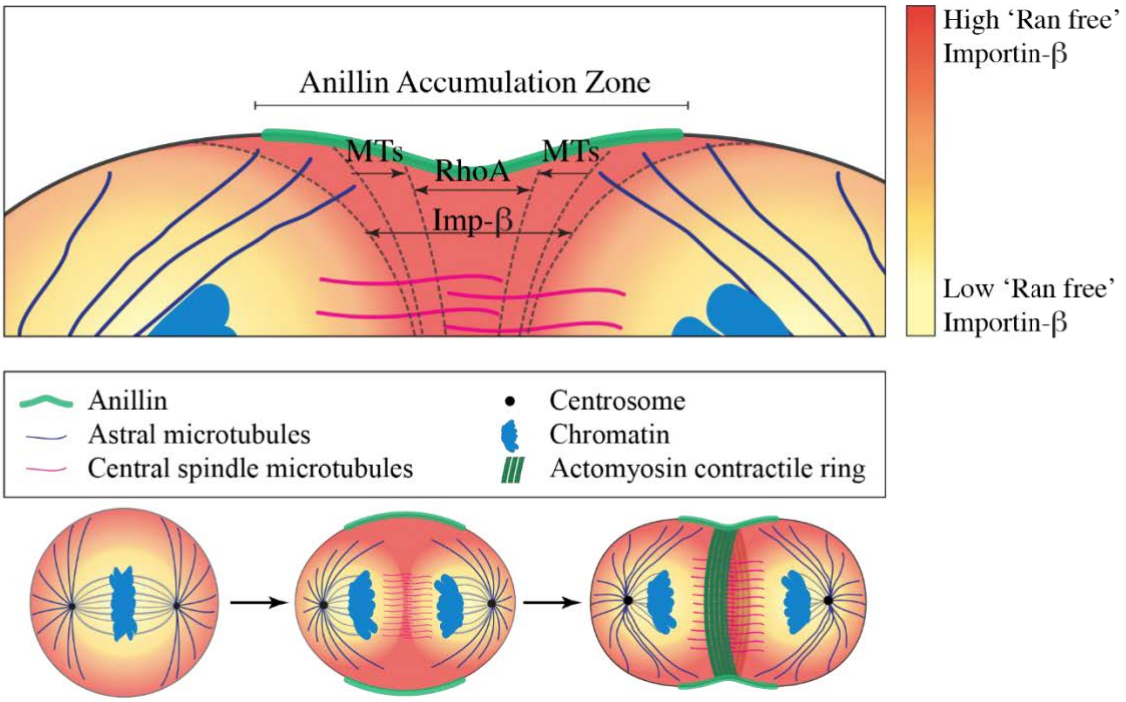
Anillin Accumulation Zone
MTs
RhoA
MTs
Imp-β
High 'Ran free' Importin-β
Low 'Ran free' Importin-β
Anillin
Astral microtubules
Central spindle microtubules
Centrosome
Chromatin
Actomyosin contractile ring

Figure 4. Importin-β gradient during cytokinesis. High importin-β gradient (dark orange) is inversely correlated with high Ran-GTP gradient (pale yellow), which is high around chromatin and low around the cortex. During anaphase, Importin-β binding mediates the recruitment of anillin (green) to the equatorial cortex. This represents the chromatin pathway that spatially coordinates anillin besides other cytokinesis pathways, including central spindle (pink) and astral microtubules (navy). The figure is adapted from (Beaudet et al., 2017).

1.5 Anillin as a target of the chromatin pathway

As described above, anillin binds to multiple components of the cell and is a key regulator of cytokinesis among metazoans (Green et al., 2012; Piekny & Glotzer, 2008; Piekny & Maddox, 2010; Figure 5). Depletion of anillin causes cytokinesis phenotypes which vary depending on the cell type and include a switch from asymmetric to symmetric ingression, oscillation of the ring due to instability in ring positioning, and failure to form a stable midbody (Hickson & O′Farrell, 2008; Maddox et al., 2007; Piekny & Glotzer, 2008; Reyes et al., 2014). In the N-terminus, anillin has a non-canonical NLS that binds to importins for nuclear localization during interphase (Chen et al., 2015). It also has binding sties for F-actin and non-muscle myosin (Figure 5; Field & Alberts, 1995; Oegema et al., 2000; Straight et al., 2005). Additional binding sites have been identified for proteins such as CD2AP, citron kinase, and mDia, among others, although it is not clear what the function of these different interactions are (El Amine et al., 2013; Haglund et al., 2010; Piekny & Maddox, 2010; Watanabe et al., 2010). Citron kinase-binding is required to retain anillin in the midbody ring, while binding to actin and myosin would crosslink the ring to the membrane via interactions in the C-terminus (El Amine et al., 2013; Gai et al., 2011; Green et al., 2012; Oegema et al., 2000; Piekny & Glotzer, 2008). In the C-terminus, anillin binds to RhoA through the RhoA-GTP binding domain (RBD), and binds to phospholipids, importin(s), microtubules and Ect2 via an adjacent C2 domain (Figure 5; Beaudet et al., 2017; Beaudet et al., 2020; Budnar et al., 2019; Frenette et al., 2012; Liu et al., 2012; Sun et al., 2015; van Oostende Triplet et al., 2014). A Pleckstrin homology (PH) domain is found at the very C-terminus, and binds to septin filaments and phospholipids (Figure 5; El Amine et al., 2013; Green et al., 2012; Liu et al., 2012; Piekny & Maddox, 2010). Anillin is recruited by active RhoA and localizes to the equatorial cortex, where it can feed back to stabilize RhoA (Beaudet et al., 2020; Budnar et al., 2019; Piekny & Glotzer, 2008). Although the mechanism is not clear, one model is that anillin promotes the clustering of $PI_{4,5}P_2$ lipids that are favored by RhoA, and this influences the residence kinetics of RhoA to increase binding to downstream effectors for ring assembly and ingression (Budnar et al., 2019). Our recent work has shed light on how inter- and intra-molecular interactions in the C-terminus help regulate anillin's function.

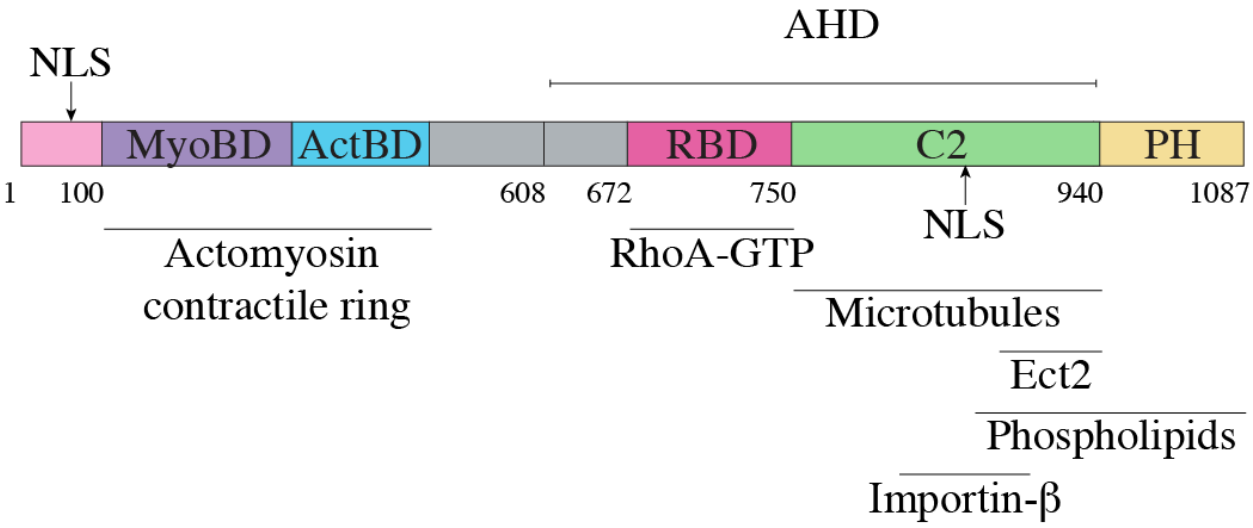

MyoBD → Myosin

ActBD → Actin

RBD → RhoA

C2 → Microtubules, Importin-β, Ect2, Phospholipids

PH → Phospholipids, Septins

Figure 5. The molecular structure of anillin. In the N-terminus, a non-canonical NLS is present to mediate the nuclear localization of anillin during interphase (pink). Myosin and actin bind to their binding domains (BD) on anillin (purple and blue, respectively) to facilitate contractile ring assembly and ingression. In the C-terminus, Anillin-homology domain (AHD) consists of RBD (magenta) and C2 domains (green). RhoA binds to RhoA-binding domain (RBD). C2 domain binds to multiple cytokinesis regulators including microtubules, Ect2, importin-beta, and phospholipids. Importin-beta binds to anillin through an NLS that exists on the C2 domain. The pleckstrin homology (PH) domain of anillin (yellow) binds to phospholipids and septins. The figure is adapted from (Beaudet et al., 2020).

Importin-binding facilitates the recruitment of anillin to the equatorial cortex (Figure 4). Our lab found that importin-beta binds to anillin through a conserved NLS in the C2 domain (Beaudet et al., 2017; Beaudet et al., 2020; Figure 5). In mammalian cells, point mutations that disrupt importin-beta binding results in delayed recruitment to the equatorial cortex, higher off-rates, and cytokinesis failure. The over-expression of importin-beta also reduces anillin's recruitment to the equatorial cortex (Beaudet et al., 2017). This observation was similar to a previous finding in Drosophila embryos, where the over-expression of importin-alpha during cellularization caused a decrease in anillin and septin (Peanut) localization (Silverman-Gavrila et al., 2008). Cellularization is the process where membranes invaginate between nuclei to form compartmentalized cells during development. The authors showed that Peanut binding to anillin was competed by importin-alpha *in vitro*, and that Ran-GTP could promote the removal of importin-alpha from anillin (Silverman-Gavrila et al., 2008). The authors proposed a model where importin-alpha is released from anillin to permit Peanut binding within the vicinity of the nuclei. The major issue with this model is that Ran-GTP would be sequestered in the closed nuclei and would not have an opportunity to compete with importin-binding. We propose that their findings support our model, where there is an optimal level of importin-binding that facilitates anillin's localization via binding to lipids and septins. If importin levels are too high, they outcompete binding to other factors that are required for anillin's cortical recruitment.

We also found that there are intramolecular interactions in the C-terminus that control anillin's function. In particular, the RhoA binding domain (RBD) autoinhibits the adjacent C2 domain, which contains the NLS (Beaudet et al., 2017; Beaudet et al., 2020). The C-terminus of anillin does not localize to the nucleus, but the C2 domain is nuclear after removal of the RBD (Beaudet et al., 2017; Beaudet et al., 2020). The C-terminus only weakly binds to importins or microtubules, but their binding to the C2 domain is much stronger after removal of the RBD (Beaudet et al., 2017; Beaudet et al., 2020). We proposed a model whereby active RhoA binds to the RBD in anaphase, to relieve the autoinhibition and expose binding sites for other components in the C-terminus.

To summarize, the Ran-GTP gradient ensures robust cytokinesis by creating an inverse gradient of importins that coordinates cortical polarity with chromatin position. This chromatin-sensing pathway works redundantly with other cytokinesis pathways in symmetrically dividing cells, and act as a back-up mechanism if other pathways are disrupted. For example, it can spatially

regulate cytokinesis if microtubules are perturbed (Beaudet et al., 2017; Kiyomitsu & Cheeseman, 2013). Previous studies showed that Ran-GTP gradient varies among cell types (Kaláb et al., 2002; Kaláb et al., 2006; Kaláb & Heald, 2008). We hypothesize that asymmetrically dividing cells, or cells with different ploidy or fate, may have stronger requirements for the Ran pathway.

1.6 The chromatin pathway and cancer cells

Cancer cells have aneuploidy and yet divide successfully despite this genomic instability. It is not known how this occurs, but studies have shown that factors controlling spindle assembly are often upregulated in cancer cells. In particular, RCC1 is overexpressed and/or upregulated in many cancers, and cancer cells have a steeper Ran-GTP gradient that correlates with increased chromosomal numbers (Hasegawa et al., 2013). They proposed a model where the steeper gradients could more strongly control spindle assembly factors, and the complexes required for kinetochore attachments. We hypothesize that the steeper Ran-GTP gradient could play a dominant role vs. microtubule-dependent pathways in positioning the contractile ring for cytokinesis of cancer cells with high aneuploidy (Figure 6). In support of this model, anillin is also overexpressed in many cancer cells including those from the liver, pancreas, breast and lung (Hall, 2005; Piekny & Maddox, 2010; Wang et al., 2020; Zhang et al., 2018). The depletion of anillin in mice delayed or prevented liver tumor progression without affecting the normal function of the liver tissue (Zhang et al., 2018). However, since hepatocytes (predominant liver cell type) typically have high ploidy due to failed cytokinesis and endoreplication, it is not clear if this would apply to other types of cancers. Our knowledge of anillin's requirement and function for cytokinesis has been limited to a handful of model systems. Depletion of anillin in HeLa cells, early *Xenopus leavis* embryos or S2 drosophila cells results in destabilization of the contractile ring and cytokinesis failure (Hickson & O′Farrell, 2008; Piekny & Glotzer, 2008; Piekny & Maddox, 2010; Reyes et al., 2014). However, depletion of ANI-1 (one of *C. elegans* anillins) in the one-cell C. *elegans* embryo causes only mild cytokinesis phenotypes where cells ingress symmetrically vs. asymmetrically and are sensitized to failure upon perturbation of other cytokinesis components (Maddox et al., 2005; Maddox et al., 2007). Interestingly, depletion of ANI-1 causes cytokinesis failure of neuroblasts during mid-embryogenesis, but not other cell types (Wernike et al., 2016). This suggests that there are different threshold requirements for anillin depending on the organism and cell type, reflecting the need to study anillin function in different contexts. We hypothesize

that there is a stronger requirement for the chromatin pathway in cancer cells with higher aneuploidy, which have steeper Ran-GTP gradients (Figure 6).

1.7 Thesis summary

To address the role of the chromatin pathway in cells with high ploidy, we characterized the requirement of anillin in different cell lines. We used immunofluorescence in multiple cell lines to determine the requirement of anillin during cytokinesis. We also generated tools to study the role of endogenous anillin in cytokinesis with higher precision than previous methods (Chapter 3). Until now, we relied on RNAi to knock down anillin, with no way of measuring the extent of knockdown in live cells. Different phenotypic severities that likely reflect different requirements could simply be due to differences in knock down efficiencies. In addition, we relied on the over-expression of exogenous constructs to determine the function of different interactions. Accordingly, we used CRISPR to generate cultured HCT 116 (colorectal cancer) cells where anillin is endogenously tagged with mNeonGreen, and performed anillin RNAi in these cells to correlate cytokinesis phenotypes with precise levels of endogenous anillin.

We also determined the molecular mechanism by which anillin is regulated for cytokinesis (Chapter 4). I helped to characterize how the region that lies at the interface of the RBD and C2 domain is required for intramolecular regulation of anillin for its function in cytokinesis. Since the phospholipid-binding and importin-binding sites are close together, I showed that mutations in the NLS that disrupt importin-binding do not disrupt phospholipid-binding. Our model is that importin-binding may stabilize an open conformation of anillin that facilitates its cortical recruitment. This requires that importin has lower affinity for anillin compared to phospholipids to support its hand-off to the membrane. Indeed, we previously found that in cells, the over-expression of importins can inhibit vs. facilitate anillin's cortical localization. In support of this, I found that importins competed with lipids for anillin-binding *in vitro*. This data provides support for our model demonstrating that importin-binding may facilitate cortical recruitment at ideal concentrations, but may inhibit anillin when it is too high, or too low.

A

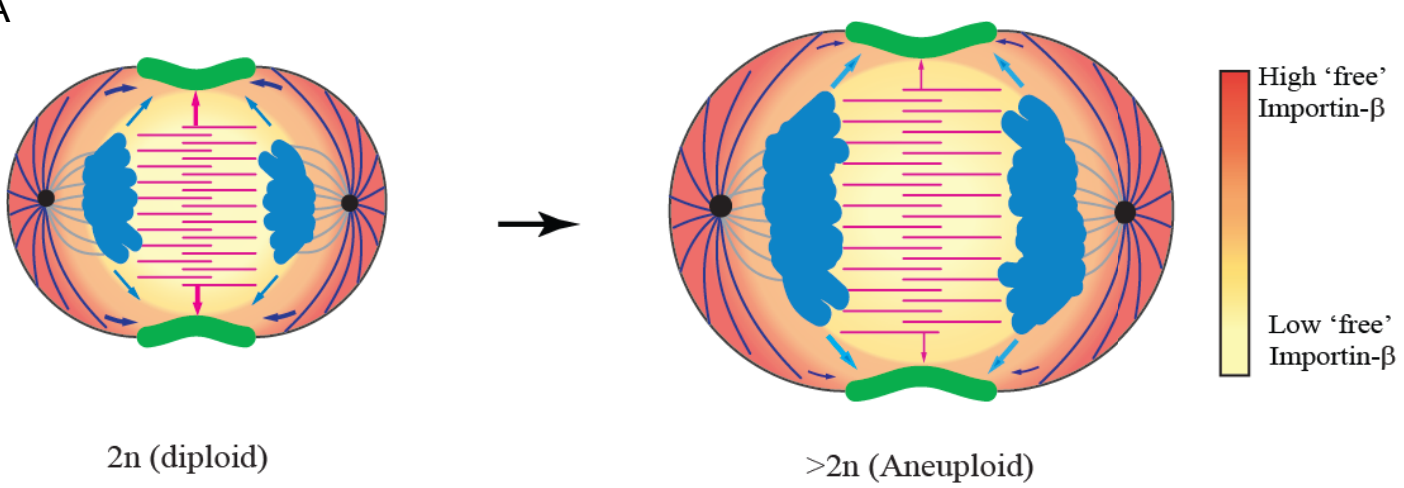
High 'free' Importin-β
Low 'free' Importin-β
2n (diploid)
>2n (Aneuploid)
Anillin
Astral microtubules
Central spindle microtubules
Centrosome
Chromatin

B

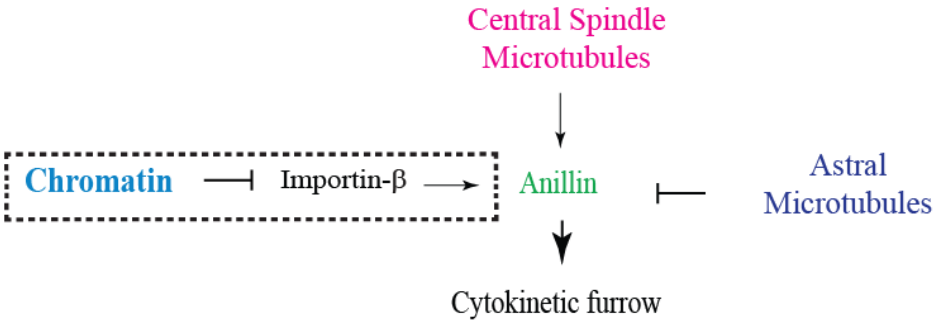
Central Spindle Microtubules
Chromatin
Importin-β
Anillin
Astral Microtubules
Cytokinetic furrow

Figure 6. The requirement of the chromatin pathway in cells with different ploidy. A. On the right, a diploid cell showing the contribution of cytokinesis pathways presented by arrows. Signals emitted from the central spindle (pink), astral microtubules (navy), and chromatin (blue) regulate cytokinesis. In a diploid cell, the pathways work redundantly to regulate cytokinesis. On the left, an aneuploid cell showing chromosomal gain (>2n). The chromatin pathway is hypothesized to be dominantly contributing to regulate cytokinesis. B. The contribution of different pathways to regulate the function and cortical recruitment of anillin. It is hypothesized that cells with higher ploidy would rely more heavily on the chromatin pathway (highlighted by a dotted box) to recruit anillin to the equatorial cortex.

Chapter 2. Materials and Methods

2.1 Cell culture

HeLa cells were grown and plated in DMEM (Wisent), supplemented with 10% cosmic calf serum (CCS; Thermo Scientific), and 2 mM L-glutamine (Wisent). HCT116 cells were grown in McCoy's Medium (Wisent) with 10% CCS. A549 cells were grown in F12K Medium (Wisent) with 10% CCS. HFF-1 cells were grown in DMEM, supplemented with 10% fetal bovine serum (FBS; Thermo Scientific). Cells were maintained in an incubator of 5% CO_2 at 37 °C.

HCT116, HeLa, A549, and HFF-1 cells were seeded on square or round (No. 1.5) coverslips in 6-well plates to reach a confluency of ~50-60%. Coverslips were acid-washed with 0.1M HCl, then washed and sterilized with isopropanol and air-dried before use. Alternatively, cells were plated to a similar confluency in a 35mm μ-dish (Ibidi). The cells were transfected with 3 uL of 2 nM of anillin siRNA using Oligofectamine (Invitrogen) as recommended by the manufacturer's protocol except we used 9 uL per well in 6-well plates. The following siRNA was used to deplete endogenous Anillin; 5'CAUAUAAGUCUAAGGAAU3' (Dharmacon) as described previously (Piekny & Glotzer, 2008). For transfection or co-transfection with DNA, 0.5-2 ug DNA was added, or combined with the siRNAs, using Lipofectamine 3000 or 2000 (Invitrogen) as recommended by the manufacturer's protocol, except that 3 uL of reagent was used to reduce lethality. Cells were fixed and/or imaged after 24-30 hours.

2.2 Plasmids

The anillin constructs tagged with GFP (GFP:Anillin; GFP:Anillin (C-terminus) for mammalian cell expression or protein expression tagged with MBP or GST (Anillin:MBP; Anillin:GST; Anillin:GST (AHD; 608-940); Anillin:GST (C-terminus; 608-1087)) were generated previously (Piekny and Glotzer, 2008; Frenette et al., 2012). Myc:Ect2 (C-terminus), 850 KK 851-DE (the NLS mutant), and A703E; E721A (the RBD mutant) were generated previously (Beaudet et al., 2017; Frenette et al., 2012). The 735 LL 736-DD (strong I/F), and the strong I/F + NLS mutants were generated in the anillin constructs by quick-change PCR. All constructs were verified by sequencing.

2.3 Fixing and immunofluorescence

Cells were fixed for immunofluorescence using TCA as previously described (Yüce et al., 2005). Specifically, cells were first washed with cytoskeletal buffer (80 mM PIPES, 1mM $MgCl_2$, 5 mM EGTA), then incubated with ice-cold 10% w/v trichloroacetic acid (TCA) at 4 °C for 14 minutes. The cells were then washed and permeabilized 4 times with 0.3% Triton X-100 phosphate-buffered saline (0.3% PBST) (pH 7.0). For immunostaining, the coverslips were placed in a chamber with wet paper towels to prevent the cells from drying. The cells were blocked with 5% Normal Donkey Serum (NDS) in PBS-T for 25 minutes prior to adding 1:200 rabbit anti-anillin (Piekny & Glotzer, 2008) or rabbit anti-GFP antibodies (generously provided by M. Glotzer, University of Chicago) and 1:400 mouse anti-alpha-tubulin (DM1A; Sigma-Aldrich) or 1:100 mouse anti-GFP (Clones 7.1 and 13.1; Roche) primary antibodies for 2 hours at room temperature. The cells were then washed 3 times with 0.3% PBS-T and incubated with 1:250 anti-mouse or anti-rabbit 488 and 1:250 anti-mouse or anti-rabbit 568 (Invitrogen) secondary antibodies for 2 hours at room temperature. The cells were then washed and incubated with 1:1000 of DAPI (1 mg/mL; Sigma-Aldrich) for 5 minutes to stain the DNA, after which they were washed once with 0.3% PBS-T followed by a final wash with 0.1 M Tris pH 8.8. After aspiration, pre-warmed mounting media (4% n-propyl gallate in 50% glycerol, 0.1 M Tris pH 8.8) was added to the cells, which were placed on glass slides and sealed by nail polish for imaging.

2.4 Microscopy

Fixed cells were imaged using two different microscopes. Cells were imaged using the Nikon Eclipse TiE inverted epifluorescence microscope with Lambda XL LED light sources. Fields of view were acquired using the 60x/1.4 Plan APO oil immersion objective (pixel size 0.27 μm), using a Piezo Z stage (ASI), a Photometrics Evolve 512 EMCCD camera and Elements acquisition software (Nikon), and a Heliphor LED-based source (405, 480, 555nm). Settings were established and kept constant based on the control samples (Figures 7 B and 8 A). Cells also were imaged using a Leica DMI6000B wide-field microscope with the 63x/1.4 PL APO oil immersion objective (pixel size 0.102 μm), and Z-stacks of 1 μm were acquired with a Hamamatsu OrcaR2 camera and Volocity software (PerkinElmer) using a Piezo Z stage (MadCityLabs) (Figure 13 B). All image files with the appropriate Z-stack were exported as TIFFs, which were opened with ImageJ (NIH). Merged colour images were then converted into 8-bit images and imported into Illustrator (Adobe) to make figures.

For live imaging, cells were incubated in the humidified incubator with 40 nM Hoechst 33342 (Invitrogen) for 30 minutes. Glass coverslips were placed on a 35mm Chamlide magnetic chamber (Quorum). The coverslips were supplemented with 1 mL of corresponding media and transferred to the INU-TiZ-F1 humidifier where the temperature of the stage was kept at 37 °C and the cover at 40 °C in presence of 5% CO2. For figure 9 C, cells were incubated with 100 nM Sir-Tubulin for 3 hours (Cytoskeleton, Inc.) to stain microtubules prior to imaging. Live imaging was done on a Ti epifluorescent microscope with a livescan Swept Field confocal unit (Nikon). A 60x with 1.4 CFI PLAN APOVC oil immersion objective (pixel size 0.27 μm) lens was used. Imaging of selected cells were set to Z-stacks, using the piezo Z stage nano-Z100 N, of 1 um for 15 steps above and below the mid-plane for every 9 minutes for 2 hours and 45 minutes (Figure 9 C and 10). The iXON897 EMCCD Camera (Andor) was used in presence of Elements acquisition software (Nikon) with a slit size of 70 μm with the 488, and 405 lasers which was set for 20% and 10%, respectively (Figure 10) in addition to the 561 nm laser which was set for 26% laser power (Figure 9 C). The exposure time was set in the control to be 200 ms; which was applied to the experimental coverslip (Figures 9 C and 10). Movies were analyzed using ImageJ and imported into Illustrator (Adobe) to make figures. For Figure 15, images were acquired using the 488 and 561 nm, lasers (100 mW, Agilent) with 200 ms exposure time which was set between 20-40% laser power, depending on the intensity of fluorescent signals (settings were kept constant for related experiments), and multiple Z-stacks of 0.5 μm or 1 μm were taken every 60 seconds per cell using NIS-Elements acquisition software (Nikon), and a narrow GFP or dual filter (500-544 and 600-665 nm; Chroma). All of the images co-expressing GFP and mRuby probes were spectrally unmixed using the NIS-Elements acquisition software (Nikon). Image files were exported as TIFFs, which were opened with ImageJ (NIH) and converted into maximum intensity Z-stack projections. Projections and merged colour images were then converted into 8-bit images and imported into Illustrator (Adobe) to make figures.

2.5 Quantification

Fixed interphase cells were used to determine the proportion of mono and binucleate cells. Data was analyzed using Excel (Microsoft) and graphed using GraphPad (Prism; Figures 7 and 8). To determine the levels of anillin remaining after RNAi for the acquired images in Figure 10, the appropriate Z-stack was opened in Image J, and a free-hand shape was drawn around the cell in

anaphase to measure the levels (a.u.) of the pixels inside the shape. The average fluorescence intensity of the entire siRNA-treated cells was divided by the average fluorescence intensity of the non-treated cells. Cells were monitored for cytokinesis phenotypes by determining the time point when furrow regression was first observed, and correlated with their levels determined as above. Data analysis was done on Excel (Microsoft) and GraphPad (Prism) to make graphs.

To determine changes of the nuclear localization for GFP:Anillin (C-term; 608-1087) and the generated (the NLS; the strong I/F; the NLS + strong I/F) mutants (Figure 13B), 2 ROI's of the nucleus and the cytosol of each interphase cell were selected. The average fluorescence intensity of the ROI of the nucleus was divided by the average ROI of the cytosol. If the ratio (*R*) was above 1.25, the localization was considered nuclear. If *R* was below 1.25, the localization was considered cytosolic (Figure 13C). All data was imported into Excel (Microsoft), where calculations were performed including standard deviations and Student's t tests. Images were transferred to Illustrator (Adobe) to make figures.

To measure the ratio of cortical accumulation vs. cytosol, the average intensity was determined in an area drawn around the cortex from one pole to the other (Figure 15). This value was then divided by the average fluorescence intensity from the average of 3 ROI's in the cytosol. Similar timepoints were selected for anaphase just before ingression based on time from anaphase onset. All data was imported into Excel (Microsoft), where calculations were performed including standard deviations and Student's t tests. All of the images and graphs were transferred to Illustrator (Adobe) to make figures.

2.6 Protein purification for binding assays

The following proteins were made from *E. coli* BL21 cells: GST, GST:Importin-β, GST:Anillin (AHD; 608-940), MBP:Anillin (RBD + C2; 672-872), and MBP:Anillin (C-term; 608-1087), GST:Anillin (AHD; strong I/F mutant; 735 LL 736-DD), GST:Anillin (AHD; NLS mutant; 850 KK 851-DE), MBP:Anillin (AHD; strong I/F mutant), MBP:Anillin (AHD; RBD mutant; A703E; E721A) were grown to OD_{600} of 0.4-0.6 at 37 °C, then 0.5 M IPTG was added for 5 hours at 28-29 °C, and 200mL was centrifuged at 4 °C for 10 minutes. Pellets were resuspended with 25 mL cold Tris-buffered saline (TBS), centrifuged, flash-frozen and stored at -80 °C. Bacteria were resuspended in lysis buffer [2.5 mM MgCl2, 50 mM Tris, 150 mM NaCl pH 7.5, 0.5% Triton X-100, 1 mM dithiothreitol (DTT), 1 mM phenylmethanesulfonyl fluoride (PMSF)

and 1 X protease inhibitors (Roche)], incubated with 1 mg/mL lysozyme on ice for 30 minutes, then sonicated three times. Extracts were incubated with pre-equilibrated amylose resin (New England Biolabs) or glutathione sepharose 4B (GE Lifesciences) for 5 hours or overnight at 4˚C with rotation. After washing with lysis buffer, beads were stored as a 50% slurry at 4˚C or eluted in equivalent volumes of 10 mM glutathione (pH 8.0) for GST constructs on ice for 2 hours. GST:Importin-β was cleaved with 1.5 nM TEV protease enzyme (generously provided by Dr. D. Kwan, Concordia University) overnight at 4 °C. Protein concentration was determined by running samples by SDS-PAGE and measuring the density of bands in comparison to known concentrations of BSA and/or by Bradford assay for eluted proteins.

To monitor protein-protein interactions, proteins from cell lysates after transfection were pulled down using the purified recombinant proteins described above. Transfected Hela cells were lysed in 50 mM Tris pH 7.6, 150 mM NaCl, 5 mM $MgCl_2$, 0.5% Triton X-100, 1 mM DTT, 1 mM PMSF with 1 X protease inhibitors (Roche) and incubated with 5-10 µg of purified MBP-tagged anillin or GST-tagged importin-β protein on beads at 4°C overnight. After binding, beads were washed 3–4 X with 50 mM Tris pH 7.6, 150 mM NaCl, 5 mM $MgCl_2$ before adding SDS sample buffer (200 mM Tris-HCl pH (6.8), 8% SDS, 0.4% Bromophenol blue, 40% glycerol, 5% β-mercaptoethanol) to denature the proteins for SDS-PAGE. Gels were wet-transferred to nitrocellulose membrane for western blotting. All blots were reversibly stained with Ponceau S to show total protein. The blots were blocked with 5% milk for 20 minutes, then incubated with either mouse anti-MBP antibodies at a dilution of 1:5000 (New England Biolabs) or 1:2500 mouse anti-GFP antibodies (see above; Roche) in 1 X PBS-T (0.140 M NaCl, 2.7 mM KCl, 10 mM Na_2HPO_4, 1.8 mM KH_2PO_4, 0.5% Triton X-100) for 1-2 hours at room temperature. After washing the membrane 3-4 X with 1 X PBS-T, 1:10000 secondary antibodies [anti-rabbit-HRP or anti-mouse-HRP (Cedarlane) were added as per manufacturer's instructions in 1 X PBS-T for 1 hour. The blots were developed using enhanced chemiluminescence (ECL) western blotting detection reagents (GE Amersham) and visualized on a GE Amersham Imager 600. All results from each pull down assay were replicated in at least three distinct experiments to ensure reproducibility.

To assess changes in anillin's interaction with phospholipids, we used PIP strips (Echelon Biosciences). The PIP strips were blocked with 3% skim milk in 0.1% 1 X TBS-T (0.1% Tween 20) at 4°C overnight. PIP strips were removed from blocking solution and incubated for 2 hours at room temperature with 1 µg/mL of purified GST (control) or one of the GST-tagged

recombinant anillin: GST:Anillin (C-term), GST:Anillin (AHD), GST:Anillin (AHD; strong I/F mutant), or GST:Anillin (AHD; NLS mutant). For Figure 16, the PIP strip was incubated with 1:1.13 molar ratio of importin-β and 1 μg/mL of the strong I/F for 2 hours at room temperature following the pre-incubation of importin-β with GST:Anillin (AHD; strong I/F mutant; 735 LL 736-DD) for 40 minutes at 4 °C. After washing 3-4 X with 1X TBS-T, the strips were incubated with 1:10000 mouse anti-GST antibodies (Sigma-Aldrich).1:10000 of the secondary antibody (anti-mouse-HRP) were then added in 1 X TBS-T for 1 hour. After washing the membranes 3-4 X with 1 X TBS-T, the signal was developed using enhanced chemiluminescence (ECL) western blotting detection reagents (GE Amersham) and visualised on a GE Amersham Imager 600. Images were converted to 8-bit by ImageJ and made into figures using Adobe Photoshop and Illustrator (Adobe).

Chapter 3. Results: Determining anillin requirements for cytokinesis

3.1 Anillin requirement varies in different cultured human cell lines

Anillin is a conserved part of the contractile ring in metazoans, but its requirement for cytokinesis seems to vary widely depending on the model organism and/or cell type. However, to our knowledge, anillin has only been studied in a few human cell lines, and most of our knowledge of human anillin function has been generated in HeLa cells (*e.g.;* Beaudet et al., 2017, 2020; Liu et al., 2012; Piekny and Glotzer, 2008; Sun et al., 2015; van Oostende Triplet et al., 2014). To determine how anillin requirement varies among different human cell types, we performed anillin knockdown by RNAi in 1) HFF-1 (human foreskin fibroblasts; modal chromosome number: 46) as a model for non-cancer diploid cells, 2) HCT116 (colorectal carcinoma; modal chromosome number: 45) as a model for a cancer cell type that has aneuploidy, but is near diploid, 3) HeLa (cervical adenocarcinoma, modal chromosome number: 82) and 4) A549 (lung carcinoma; modal chromosome number: 66) as cancer cell types with aneuploidy and high net chromosomal numbers. We used a fixed-cell immunofluorescence assay to monitor endogenous anillin expression and cytokinesis phenotypes in population of cells. In particular, when cells fail cytokinesis, they become binucleate, which can be easily visualized using a stain for DNA. We also performed a western blot on a population of cells to determine that the levels of anillin were knocked down to similar levels among the cell lines. As shown in Figure 7A, anillin levels were drastically reduced in all four cell lines compared to the control cell populations. Staining of individual cells also revealed a strong reduction in anillin, which is typically nuclear localized in interphase cells (Figure 7B). Despite the similar knockdown between different cell lines, we observed differences in the proportion of cells that failed cytokinesis. While 22.5% of HFF-1 and 20.3% of HCT116 cells were binucleate (compared to 2.7% and 7.2% binucleate in the control populations, respectively), 63.4% of HeLa and 47.1% of A549 cells were binucleate (Figure 7C). This suggests that different types of human cells have different requirements for anillin to support successful cytokinesis. In particular, HeLa and A549 cells with higher modal chromosome numbers had stronger requirements compared to those with lower numbers, even though HCT 116 cells are cancerous and have aneuploidy. This experiment was verified by Kamar Raad and I using

an analogous approach, where we measured and quantified the breadth of anillin and counted binucleate cells in the different cell lines.

3.2 Anillin requirement in HCT 116 cells increases with ploidy

We found it intriguing that anillin's requirement for cytokinesis varies between different cell types. We propose that anillin, as a target for the chromatin sensing pathway, could be more required in cells with higher ploidy because they rely more on this pathway for cytokinesis. However, these different requirements could be due to differences in their genetic backgrounds. Therefore, we determined if anillin's requirement for cytokinesis increases in the same cell line when ploidy is increased. To do this, we treated HCT 116 cells with cobalt II chloride ($CoCl_2$), a hypoxia mimicking agent previously shown to induce an increase in ploidy (Lopez-Sánchez et al., 2014). A mixed population of cells was treated with anillin siRNAs, then the cells were fixed and monitored for cytokinesis failure by counting the proportion of binucleate cells that were: 1) similar in size to the parent population, or 2) at least 2-fold larger in size (Figure 8A). Indeed, while 11.1% of HCT 116 cells of 'normal' size were binucleate, 38.7% of large HCT 116 cells were binucleate (Figure 8B). Therefore, the larger HCT 116 cells, which we infer have higher ploidy because cells have been shown to scale their size with ploidy (Storchova & Pellman, 2004), have a stronger anillin requirement for cytokinesis compared to cells with lower ploidy.

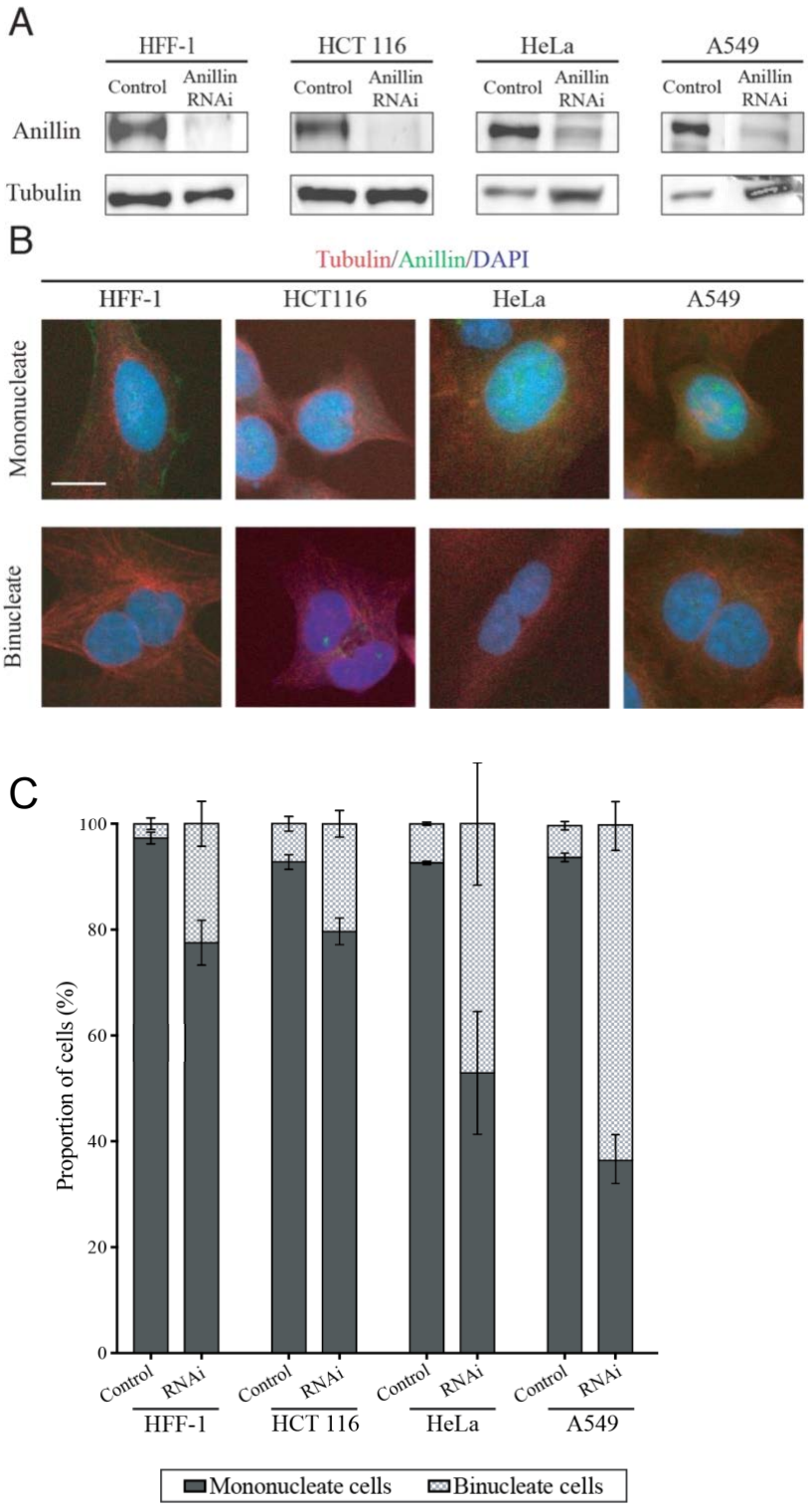
A
HFF-1
HCT 116
HeLa
A549
Control
Anillin RNAi
Anillin
Tubulin
B
Tubulin/Anillin/DAPI
HFF-1
HCT116
HeLa
A549
Mononucleate
Binucleate
C
Proportion of cells (%)
100
80
60
40
20
0
Control
RNAi
HFF-1
HCT 116
HeLa
A549
Mononucleate cells
Binucleate cells

Figure 7. Anillin requirement varies among different cultured human cell lines. A. Western blots show the knockdown of anillin (top panels) in HFF-1, HCT 116, HeLa and A549 cells, with tubulin (bottom panels) used as a control to compare loading. B. Images show fixed cells co-stained for tubulin (red), anillin (green), and DNA (blue) as indicated. The top panels show control cells, which are mononucleate, while the bottom panel shows cells after anillin RNAi, and are binucleate. The scale bar is 10 μm. C. A bar graph shows the percentage of mononucleate and binucleate cells representing cytokinesis success vs. failure, respectively, for each of the cell lines as indicated. For each cell type, 300-400 cells were quantified (N=3 replicates) for control vs. RNAi-treatment. Bars show standard deviation. Dr. Su Pin Koh, Brandon Jaunky and Kevin Larocque contributed to the experiments.

A

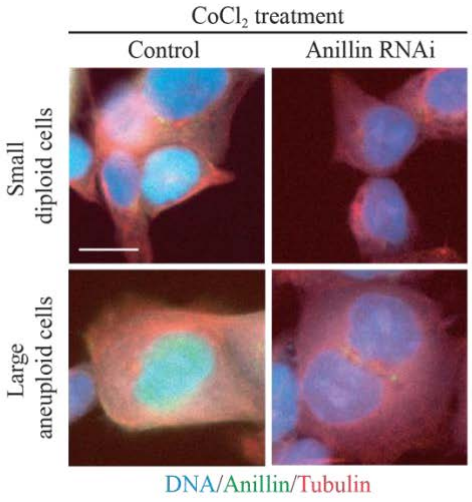
CoCl2 treatment
Control
Anillin RNAi
Small diploid cells
Large aneuploid cells
DNA/Anillin/Tubulin

B

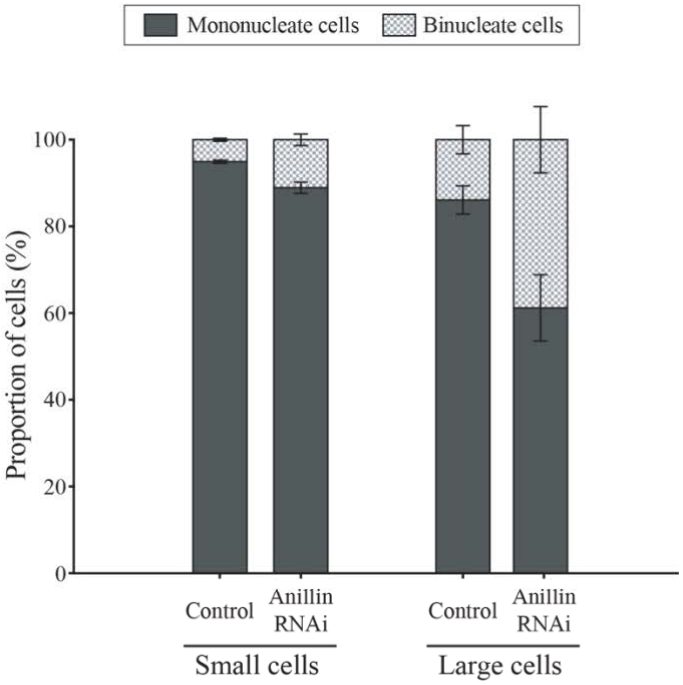
Mononucleate cells
Binucleate cells
Proportion of cells (%)
100
80
60
40
20
0
Control
Anillin RNAi
Control
Anillin RNAi
Small cells
Large cells

Figure 8. Anillin requirement for cytokinesis increases with ploidy. A. Images show fixed HCT 116 cells co-stained for tubulin (red), anillin (green) and DNA (blue). Cells treated with $CoCl_2$ were either small (original ploidy) or large (higher aneuploidy). The left column shows control cells and the right column shows cells after anillin depletion. The scale bar is 10 μm. B. A bar graph shows the proportion of mononucleate (successful cytokinesis) and binucleate (failed cytokinesis) $CoCl_2$ -treated small or large HCT 116 cells for control vs. anillin RNAi. For each treatment, 300 cells were quantified (N = 2 replicates for control, N = 3 replicates for anillin RNAi). The bars show standard deviation. Experiments were done by Dr. Su Pin Koh and Kevin Larocque.

3.3 Tagging endogenous anillin in HCT116 cells

While our data supports different anillin requirements for cytokinesis in different cell types and with different ploidy, there were several caveats to this data. Western blots can report for RNAi efficiency in a population of cells, but not individual cells where it can be more variable. Immunofluorescence can report more accurately for RNAi efficiency within individual cells, but requires cells to be fixed and stained, which can introduce variability and artefacts, and only reflects an 'end-point' of cytokinesis failure. To overcome this problem, we endogenously tagged anillin in HCT 116 cells with the fluorescent protein mNeonGreen using CRISPR-Cas9. The methodology to do this is shown in Figure 9A and B. The target site that was used as the guide is shown in red, while the mNeonGreen sequence is shown in green, and the anillin coding region is shown in blue. The repair template used to insert mNeonGreen is shown along with anillin homology arms on either side of the insert. Potential clones were recovered, screened for homozygosity and sequenced to ensure that the fluorescent protein was properly incorporated without introducing mutations. The localization of endogenous mNeonGreen-tagged anillin localized similar to what we had previously described for the localization of anillin via antibody staining in fixed cells, and for transgenic probes in other cultured human cell lines (Figure 9C; (Beaudet et al., 2017, 2020; Piekny & Glotzer, 2008; van Oostende Triplet et al., 2014)). Anillin accumulates at the equatorial plane during mid-late anaphase, and subsequently to the ingressing contractile ring and midbody (Figure 9C). This localization is in line with prior experiments showing its requirement in contractile ring positioning, ingression and in midbody formation (Beaudet et al., 2017, 2020; Field & Alberts, 1995; Hickson & O′Farrell, 2008; Liu et al., 2012; Oegema et al., 2000; Piekny & Glotzer, 2008).

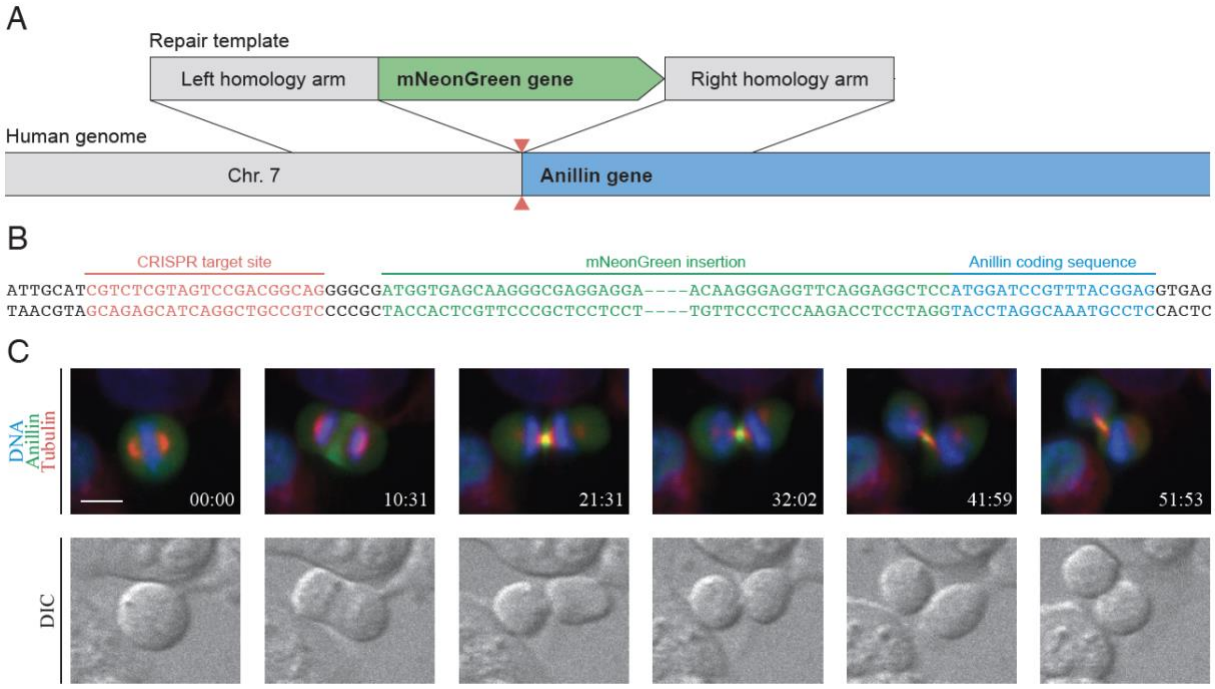
A
Repair template
Left homology arm
mNeonGreen gene
Right homology arm
Human genome
Chr. 7
Anillin gene
B
CRISPR target site
mNeonGreen insertion
Anillin coding sequence
ATTGCATCGTCTCGTAGTCCGACGGCAGGGGCGATGGTGAGCAAGGGCGAGGAGGA----ACAAGGGAGGTTCAGGAGGCTCCATGGATCCGTTTACGGAGGTGAG
TAACGTAGCAGAGCATCAGGCTGCCGTCCCCGCTACCACTCGTTCCCGCTCCTCCT----TGTTCCCTCCAAGACCTCCTAGGTACCTAGGCAAATGCCTCCACTC
C
DNA
Anillin
Tubulin
00:00
10:31
21:31
32:02
41:59
51:53
DIC

Figure 9. Endogenous tagging of anillin in HCT116 with a fluorescent protein. A. A schematic that shows the insertion of the repair template containing mNeonGreen gene using CRISPR-Cas9 approach into the human genome at the N-terminus of ANLN gene. The insertion happens following the Cas9 cleavage at the CRISPR target site which is represented by red arrows. B. DNA sequence of the CRISPR target site shown in red, the mNeonGreen DNA sequence shown in green and Anillin coding sequence shown in blue. C. Time lapse images of endogenously tagged anillin HCT116. Tubulin is shown in red (Sir-Tubulin), Anillin in green and DNA in blue (Hoechst). Times are shown in minutes and seconds. The scale bar is 10 μm. In collaboration with Mathieu Husser.

3.4 A defined threshold of anillin is required to support cytokinesis in HCT 116 cells

With a tool in hand to measure endogenous anillin, we next wanted to use this tool to determine anillin's requirement in HCT 116 cells with more temporal and spatial precision. Cells were imaged approximately 24 hours after anillin depletion, when levels are optimally reduced (Piekny & Glotzer, 2008). We imaged metaphase cells every 9 minutes, and for up to 3 hours to ensure we would capture the completion of cytokinesis. I observed two cytokinesis failure phenotypes when anillin levels were considerably reduced in cells, with examples of each phenotype shown in Figures 10 A and B. In a subset of cells, the ring ingressed but regressed soon after ingression, while in the other subset the ring remained ingressed for an extended period of time and subsequently regressed (Figure 10). I quantified this data to determine if there was a correlation with anillin levels and the severity of the phenotype observed. As expected, 100% of control cells successfully completed cytokinesis (n=50). After performing anillin RNAi (n=59), I found that as long as cells had levels of anillin >15%, they could undergo successful cytokinesis (n=16/59; representing 27% of anillin RNAi treated cells) (Figure 11A). However, when cells had <15% anillin (n=43/59), 51% cells failed cytokinesis (n=30/59) and 22% succeeded cytokinesis (n=13/59; Figure 11A). Of the cells that failed cytokinesis, 23% had the early regression phenotype, while 77% showed the late regression phenotype (Figure 11B). Interestingly, when the anillin levels were measured specifically in cells that had <15% anillin (n=43), there was no difference in the remaining levels and cytokinesis failure phenotypes observed (Figure 11C). For example, cells with <2% remaining anillin showed early or late regression (Figure 11C). The mononucleate cells with <15% anillin that succeeded cytokinesis, had at least 5% anillin (Figure 11C). Therefore, we now know that the absolute threshold amount of anillin required to support cytokinesis in HCT 116 cells is 5%, and the ideal threshold is above 15%. This precise way of measuring anillin's requirement for the different stages of cytokinesis can help us determine how changing ploidy alters this requirement, and how it varies between cell types.

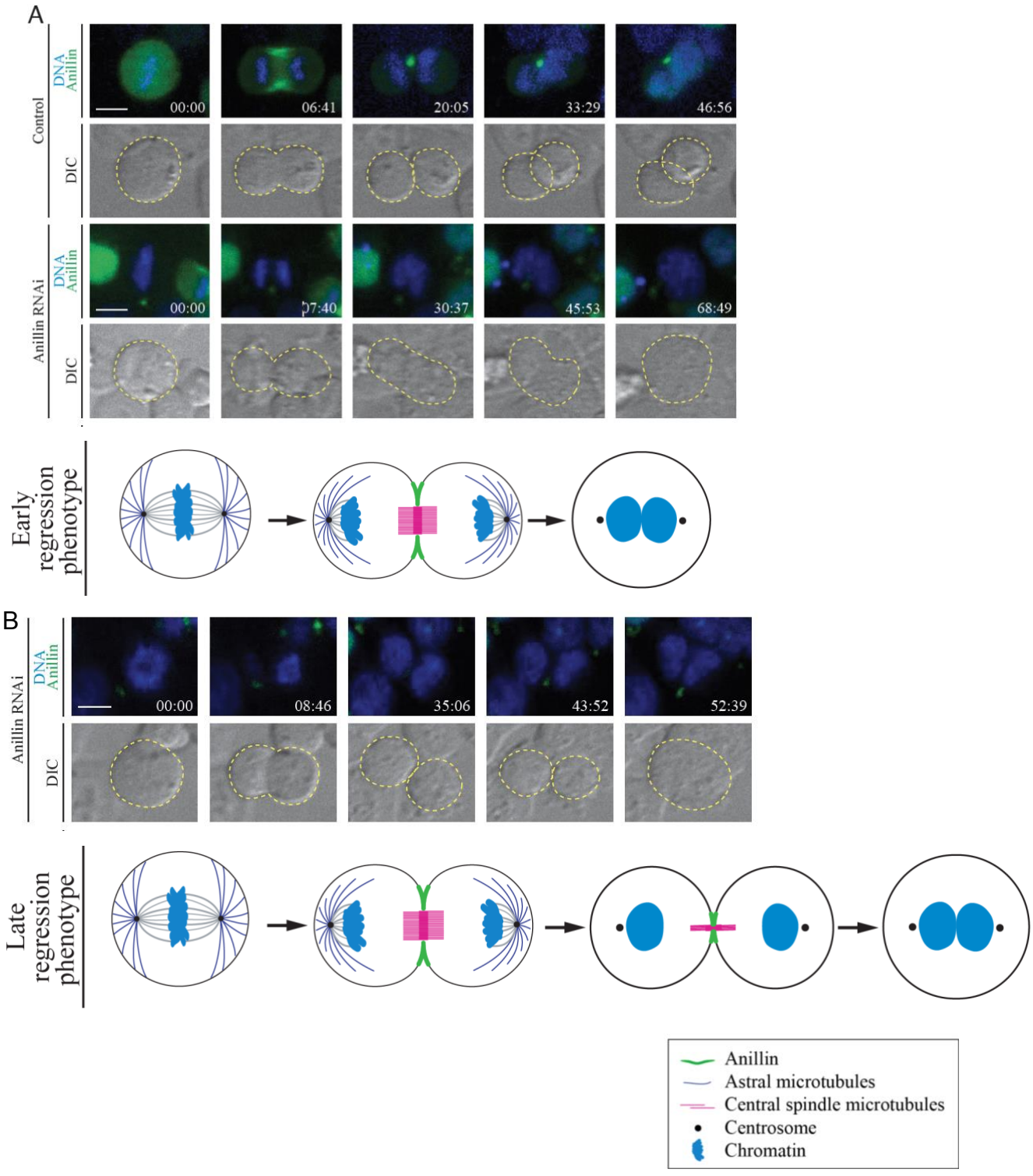
A
Control
DNA
Anillin
DIC
00:00
06:41
20:05
33:29
46:56
Anillin RNAi
DNA
Anillin
DIC
00:00
07:40
30:37
45:53
68:49
Early regression phenotype
B
Anillin RNAi
DNA
Anillin
DIC
00:00
08:46
35:06
43:52
52:39
Late regression phenotype
Anillin
Astral microtubules
Central spindle microtubules
Centrosome
Chromatin

Figure 10. Different cytokinesis phenotypes occur in anillin-depleted HCT 116 cells. A. Time-lapse images show endogenously tagged HCT 116 cells where anillin is shown in green and DNA is shown in blue (stained with Hoechst), with DIC images of the cell underneath (cell outlined in yellow-dotted line). The times are shown in minutes and seconds. The top panel shows a control cell, and the bottom panel shows an anillin-depleted cell, with the early regression phenotype. Cartoon schematics show the early regression phenotype where the ring regresses shortly after ingression (chromatin in blue, astral microtubules in purple, central spindle microtubules in pink, contractile ring in green and centrosomes in grey). B. The top panel shows the same control cell as in A. The bottom panel shows another anillin-depleted cell that shows the late regression phenotype. Cartoon schematics show the late regression phenotype where the ring regresses after an extended period of time. The scale bar is 10 μm.

A

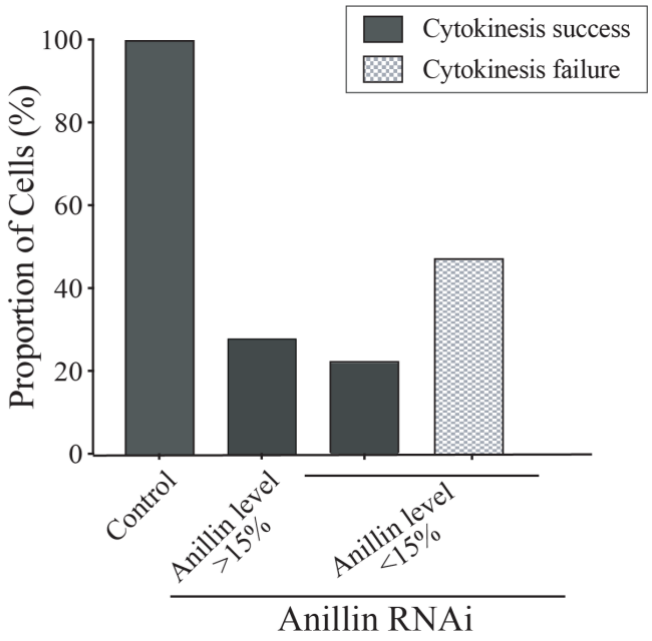
Cytokinesis success
Cytokinesis failure
Proportion of Cells (%)
100
80
60
40
20
0
Control
Anillin level >15%
Anillin level <15%
Anillin RNAi

B

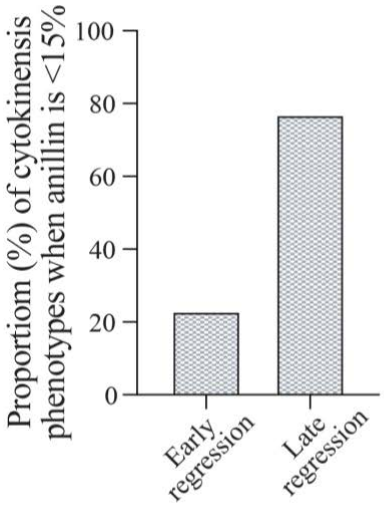
Proportiom (%) of cytokinensis phenotypes when anillin is <15%
100
80
60
40
20
0
Early regression
Late regression

C

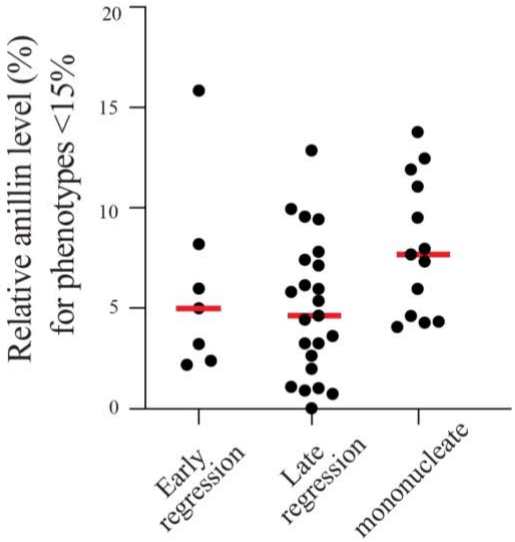
Relative anillin level (%) for phenotypes <15%
20
15
10
5
0
Early regression
Late regression
mononucleate

Figure 11. Threshold levels of anillin are required for cytokinesis in HCT 116 cells. A. A bar graph shows the proportion of control (n=50) or anillin-depleted cells that succeeded or failed cytokinesis with > 15% anillin levels, or 15% or less of anillin levels (n= 59). B. A bar graph shows the proportion of early regression (23%) and late regression (77%) phenotypes in cells that failed cytokinesis from A. C. A scatter plot shows the relative levels of anillin for individual cells with <15% anillin that showed mononucleate, early, or late regression phenotypes (n=43).

Chapter 4. Results: Determining the mechanism by which the chromatin pathway regulates anillin function for cytokinesis

***Some of this data was published in: Beaudet et al., 2020.**

We found that a chromatin-sensing pathway regulates cytokinesis by controlling contractile ring positioning. Anillin contains a conserved NLS in its C-terminus that binds to importin-beta, and mutating this site and disrupting this binding prevents anillin's cortical recruitment during anaphase, and causes cytokinesis phenotypes. We also found that there is intramolecular inhibition between the RBD (RhoA-binding domain) and neighbouring C2 domain where the NLS is located, along with binding sites for other proteins and components of the cell including phospholipids and microtubules. Our model is that RhoA-GTP binding is required to make the C2 domain accessible for binding to its interactors, which would ensure that anillin function is temporally coordinated with cell cycle exit and when Ect2 becomes active. Then, importin-binding helps stabilize this open conformation of anillin, which hands-off to phospholipids or microtubules that likely have a higher affinity for anillin. To test this, we needed to demonstrate that mutating the NLS does not directly impact phospholipid binding per se, since both regions contain basic residues and are close together. Then, we asked if the amino acids that lie at the interface between the RBD and C2 domains are required for interactions in the C2 domain, and the importance of controlling this interface for anillin function.

4.1 Mutating the NLS does not affect phospholipid-binding

Previous studies showed that the C2 domain can bind to $PI_{4,5}P_2$ phospholipids (Sun et al., 2015; Budnar et al., 2019). Because the NLS is in close proximity to the putative lipid-binding site, which also relies on a stretch of basic residues, we wanted to ensure that mutations in the NLS did not disrupt lipid-binding. I compared the phospholipid-binding profiles of recombinant control GST:anillin RBD + C2 domains, with the NLS mutant (850 KK 851-DE) and GST:anillin C-terminus (RBD+C2+PH domains) using strips blotted with a variety of lipids including mono, di-, and triphosphorylated (3,4,5) phospholipids. As shown in Figure 12, I saw an enrichment of binding to PI_3P, PI_4P and PI_5P, with weak signals at $PI_{3,5}P2$, $PI_{4,5}P_2$ and $PI_{3,4,5}P_3$. The NLS mutant retained binding to the same lipids, supporting that these mutations do not disrupt the phospholipid-binding site. However, we were surprised to see enrichments of anillin that included

PI_3P, PI_4P, PI_5P and $PI_{3,5}P_2$, which had not been previously reported. We previously saw that the C-terminus of anillin collected from cell lysates bound preferentially to $PI_{3,4}P_2$, $PI_{4,5}P_2$ and $PI_{3,4,5}P_3$ (Frenette et al., 2012). To our surprise, adding the PH domain, by testing the binding of anillin C-terminus to phospholipids, had no effect on the observed lipid profile. In the cell, anillin is bound to RhoA, which has a preference for $PI_{4,5}P_2$ lipids (although we previously also saw binding to $PI_{3,4}P_2$ and $PI_{3,4,5}P_3$; Budnar et al., 2019; Frenette et al., 2012; Liu et al., 2012; Sun et al., 2015), which could influence anillin's accessibility to this pool vs. other lipids.

4.2 Mutations at the interface of RBD and C2 domains relieve the autoinhibition of the C2 domain by the RBD

RhoA and importin binding have been shown to mediate the cortical recruitment of anillin (Beaudet et al., 2017; Budnar et al., 2019; Piekny & Glotzer, 2008). However, how RhoA and importin-binding are coordinated for the recruitment of anillin is unclear. As described above, the RBD autoinhibits the adjacent C2 domain, and we propose that RhoA-binding is required to relieve this inhibition and make the C2 domain accessible to importin-binding, which in turn stabilizes the open conformation of anillin. To test this, we created point mutations in residues found at the interface of the RBD and C2 domain (735LL736-DD; strong interface (I/F) mutant; Figure 13A). Based on their position, these mutations should reduce binding between the αB helix and the C2 domain to strongly disrupt the interface, without affecting RhoA-binding (Figure 13A; Sun et al., 2015).

First, we assessed how the strong I/F mutations affect autoinhibition of the NLS in the C2 domain. To do this, we measured changes in the nuclear localization of different anillin C-terminal constructs in interphase HeLa cells. We previously showed that the C-terminus of anillin is not localized to the nucleus during interphase, but is after removal of the RBD (Beaudet et al., 2017). I compared the distribution of GFP-tagged C-terminus anillin in interphase cells with constructs containing mutations in the NLS, the strong I/F mutant, or both (Figure 13B). Based on relative levels, their distribution was categorized as nuclear or cytosolic. In particular, nuclear localization was determined by the ratio of the average fluorescence intensity of anillin in the nucleus over the average intensity of anillin in the cytosol, where $R > 1.25$ was considered to be "nuclear" and $R < 1.25$ was considered to be "cytosolic" (Figure 13C). As shown previously, the C-terminus localized primarily to the cytosol in interphase cells, supporting the autoinhibition model (0%

nuclear). As expected, mutating the NLS did not change this localization pattern (0% nuclear). However, the strong I/F mutant localized to the nucleus in 64% of the cells, which reverted back to the cytosol when the NLS was also mutated (0% nuclear; Figure 13B). Therefore, introducing the strong I/F mutations were sufficient to relieve autoinhibition of the C2 domain from the RBD, making it accessible for importin-binding and nucleocytoplasmic transport.

4.3. The strong interface mutant causes anillin to have an open conformation

Next, we determined if the strong I/F mutant causes anillin to have binding properties similar to anillin in the presence of active RhoA. As described above, our model is that active RhoA binding relieves inhibition of the neighbouring C2 domain, and some of our data supports that mutations at the interface similarly relieve this autoinhibition. Using recombinant purified MBP:anillin (RBD + C2), the RBD mutant (A703E; E721A – predicted to no longer bind to active RhoA; Sun et al., 2015) as a negative control, or the strong I/F mutant, GFP-tagged importin-beta was pulled down from cell lysates where the levels of endogenous active RhoA were manipulated (Figure 14A). Since Ect2 is the GEF for RhoA, active RhoA was generated by overexpression (O/E) of the C-terminus of Ect2 that contains the GEF region [Myc:Ect2 (C-term)], and active RhoA was reduced by Ect2 RNAi. In both conditions, Importin-binding was higher for control anillin vs. the RBD mutant, showing the importance of RhoA-binding in altering anillin's affinity for importin. Interestingly, the strong I/F mutant bound even more strongly to importin than the control. This data suggests that the strong I/F mutant no longer requires RhoA-binding for increased accessibility to the NLS of the C2 domain, supporting a model where this mutant causes anillin to have a more open conformation (Figure 14B).

A

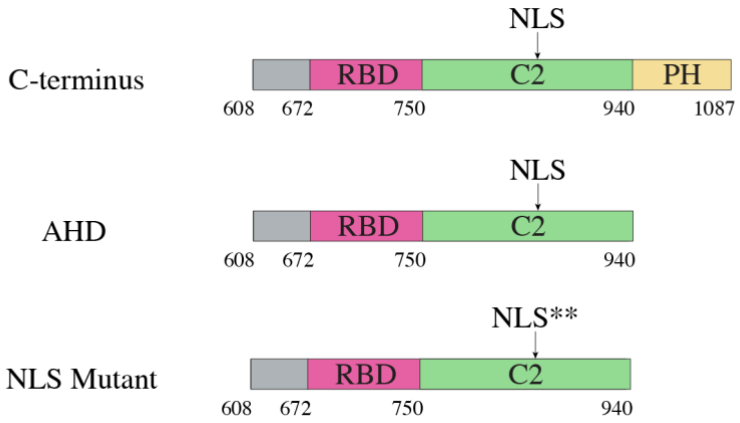
C-terminus
NLS
RBD
C2
PH
608
672
750
940
1087
AHD
NLS
RBD
C2
608
672
750
940
NLS Mutant
NLS**
RBD
C2
608
672
750
940

B

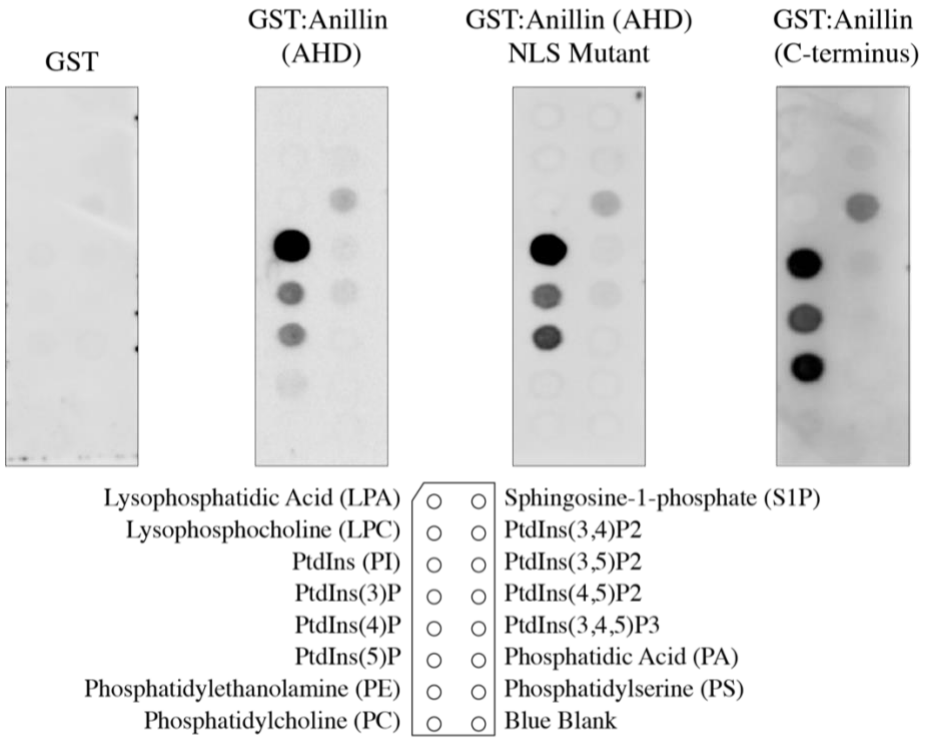
GST
GST:Anillin (AHD)
GST:Anillin (AHD) NLS Mutant
GST:Anillin (C-terminus)
Lysophosphatidic Acid (LPA)
Lysophosphocholine (LPC)
PtdIns (PI)
PtdIns(3)P
PtdIns(4)P
PtdIns(5)P
Phosphatidylethanolamine (PE)
Phosphatidylcholine (PC)
Sphingosine-1-phosphate (S1P)
PtdIns(3,4)P2
PtdIns(3,5)P2
PtdIns(4,5)P2
PtdIns(3,4,5)P3
Phosphatidic Acid (PA)
Phosphatidylserine (PS)
Blue Blank

Figure 12. Mutating the NLS does not alter recombinant anillin's binding to phospholipids. A. Cartoons show the domains of the anillin constructs; Anillin C-terminus [608-1087; RBD (pink)+C2 domain (green)+PH domain (yellow)], Anillin AHD (608-940; RBD+C2), and NLS mutant (AHD-RBD+C2 indicated by ** on the cartoon; 850 KK 851-DE). B. Images show immunoblots of PIP strips after incubation with either purified GST, which was used as a negative control (left), recombinant purified GST-tagged anillin (AHD – RBD + C2; middle left), or with the NLS mutant (AHD – RBD + C2; 850 KK 851-DE; middle right), and recombinant purified GST-tagged anillin (C-terminus–RBD+C2+PH; right). The schematic underneath shows the positions of the different lipids spotted on the strips.

A

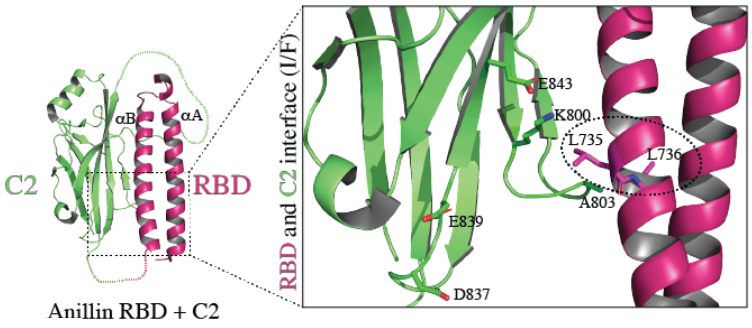

Control Anillin (NLS blocked)

strong I/F mutant Anillin (NLS exposed)

^^ *strong* I/F mutations 735LL736- DD

B

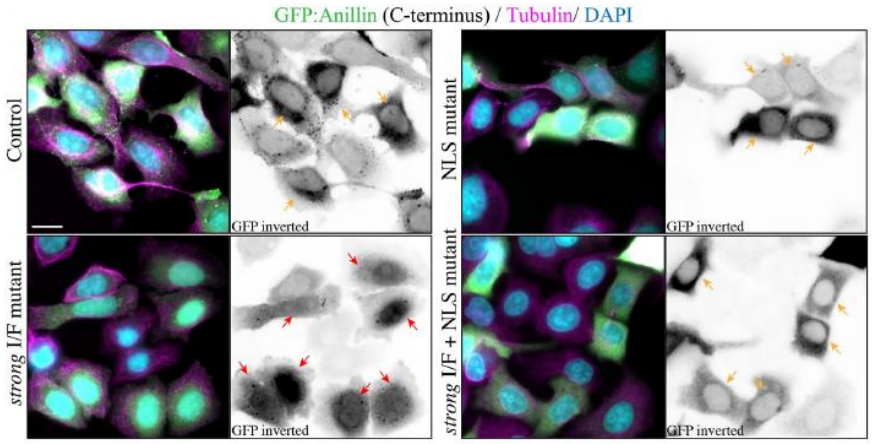

GFP:Anillin (C-terminus)	→ Cytosolic	→ Nucleus
Control	100%	0.0%
NLS mutant	100± 0% n.s.	0.0 ± 0% n.s.
strong I/F mut.	36± 0.19% ***	64 ± 0.19% ***
strong I/F + NLS mut.	100± 0% n.s.	0.0 ± 0% n.s.

C

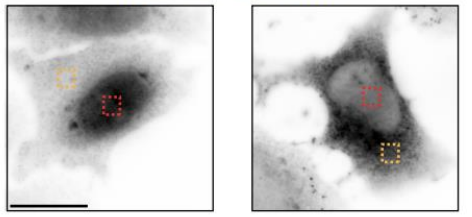

R > 1.25 = Nuclear R < 1.25 = Cytosolic

Average Nuclear GFP ROI

Average cytosolic GFP ROI

$$R = \frac{\text{Average Nuclear ROI (Red)}}{\text{Average Cytosol ROI (Yellow)}}$$

Figure 13. The strong I/F mutant relieves autoinhibition between the RBD and C2 domains. A. A ribbon structure shows the intramolecular interface between the RBD (magenta) and the C2 domain (green). The boxed inset shows the amino acids that form electrostatic and hydrophobic interactions at the interface. The amino acids that were mutated to generate a strong I/F mutant are positioned in the αB helix and are circled (L735D; L736D). To the right is a cartoon schematic illustrating how strong I/F mutations are predicted to disrupt the structure of anillin. B. Images show fixed HeLa cells expressing GFP-tagged anillin C-terminus, or the NLS mutant, strong I/F mutant, or strong I/F + NLS mutant, stained for GFP (green), tubulin (magenta), and DNA (DAPI; blue). Yellow arrows point to cytosol localization, while red arrows point to nuclear localization. To the right, the percentage of cytosolic vs. nuclear localization is indicated for each condition. Standard deviations are shown (N = 3 replicates, with n = 100–130 cells per replicate for each condition) and significance was determined using the unpaired Student's t test (n.s., not significant; ***, $p < 0.0001$). C. Inverted images of fixed interphase HeLa cells immunostained for GFP show how anillin was determined to be nuclear vs. cytosolic. The average levels in the red square (nucleus) were calculated as a ratio R vs. the average levels in the yellow square (cytosol). If $R > 1.25$, anillin was determined to be nuclear, while $R < 1.25$ was cytosolic. The scale bar is 10 μm.

A

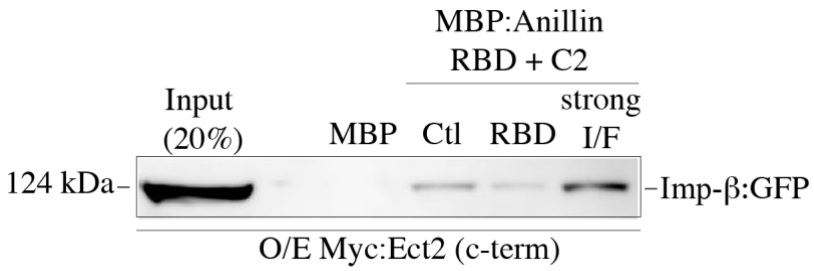
MBP:Anillin
RBD + C2
Input
(20%)
MBP
Ctl
RBD
strong
I/F
124 kDa–
–Imp-β:GFP
O/E Myc:Ect2 (c-term)

B

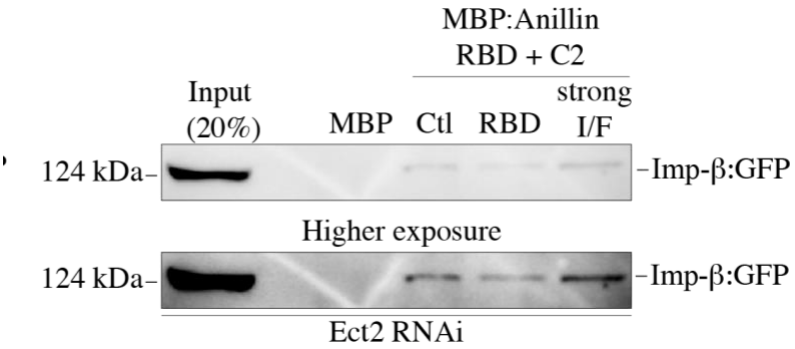
MBP:Anillin
RBD + C2
Input
(20%)
MBP
Ctl
RBD
strong
I/F
124 kDa–
–Imp-β:GFP
Higher exposure
124 kDa–
–Imp-β:GFP
Ect2 RNAi

C

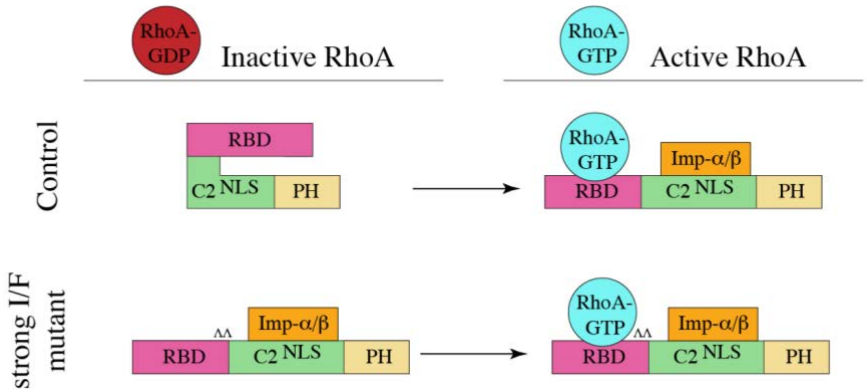
RhoA-
GDP
Inactive RhoA
RhoA-
GTP
Active RhoA
Control
RBD
C2
NLS
PH
RhoA-
GTP
Imp-α/β
RBD
C2
NLS
PH
strong I/F
mutant
Imp-α/β
RBD
C2
NLS
PH
RhoA-
GTP
Imp-α/β
RBD
C2
NLS
PH

Figure 14. The strong I/F mutant has higher affinity for importin-beta. A. An immunoblot showing pull downs of GFP-tagged importin-β from cell lysates overexpressing (O/E) Myc-tagged Ect2 C-terminus to generate active RhoA. with purified MBP or MBP-tagged anillin (RBD + C2; Ctl) or with RBD mutations that disrupt RhoA binding, or mutations that strongly disrupt the RBD-C2 interface (the strong I/F mutant). B. An immunoblot showing pull downs of GFP-tagged importin-β after Ect2 RNAi to reduce active RhoA, with purified MBP or MBP-tagged anillin (RBD + C2; Ctl) or with the RBD mutations or the strong I/F mutant. C. A cartoon schematic shows how RhoA-GTP (blue) binding to the RBD (magenta) relieves inhibition of the C2 domain (green; NLS is indicated) to enable importin-α/β (orange) binding to the NLS (PH domain is in yellow). Mutations that strongly perturb the intramolecular interface (strong I/F mutant) remove autoinhibition of the RBD, causing importin to bind more strongly to anillin regardless of RhoA binding. I helped perform parts of the experiment with Daniel Beaudet and Nhat Pham.

4.4 The interface between the RBD and C2 domain is required for anillin's cortical recruitment and function during cytokinesis

Next, we determined how disrupting the interface affects the localization and function of anillin during cytokinesis. To do this, we imaged HeLa cells depleted of endogenous anillin and co-expressing mCherry:tubulin and RNAi-resistant GFP-tagged full-length anillin as a control or containing the strong I/F mutations during cytokinesis (Figure 15). Full-length anillin localized similar to the C-terminus as previously described and all cells completed ingression (100%), while the strong I/F mutant failed to localize to the cortex and 62.5% of the cells failed to ingress (Figure 15). This data shows that the strong I/F mutations abolished anillin's recruitment to the cortex, and failed to support anillin's function during cytokinesis. Since we previously observed that the overexpression of importin-beta caused a decrease in anillin's cortical localization, we propose that the stronger affinity for importin-beta-binding to the strong I/F mutant makes it unable to compete with phospholipids for its localization at the membrane.

4.5. Importin-beta binding seems to decrease the affinity of anillin for phospholipids

Our data shows that residues interface between the RBD and the C2 domain are required to control anillin's cortical recruitment and function during cytokinesis. Our model for how importin-binding regulates anillin's localization and function is that it stabilizes an open conformation, but binds with relatively low affinity that permits hand-off to other interactors. We found that the strong I/F mutant binds more strongly to importin-beta compared to control anillin, which could out-compete anillin's ability to bind to these other interactors. In particular, RhoA and phospholipids bind cooperatively to anillin to facilitate its cortical enrichment, and if importins out-compete binding to phospholipids, this would prevent anillin's cortical accumulation. To test this model, I determined if the strong I/F mutant had a different affinity for phospholipids in the presence of importin-beta. Using the lipid strips described earlier, I added recombinant purified GST-tagged anillin (RBD + C2) with the strong I/F mutations and found that the phospholipid binding profile was similar to what I had seen with control anillin (Figures 12 and 16). However, pre-incubation of the strong I/F mutant with recombinant purified importin-beta caused ~43% decrease in its affinity for PI_5P (Figure 16). Although preliminary, this data suggests that importin-beta binding to the strong I/F could compete with anillin to binding to phospholipids, and supports a model where optimal importin-binding facilitates anillin function, but tipping the balance of this binding (*e.g.* too low or too high) is detrimental.

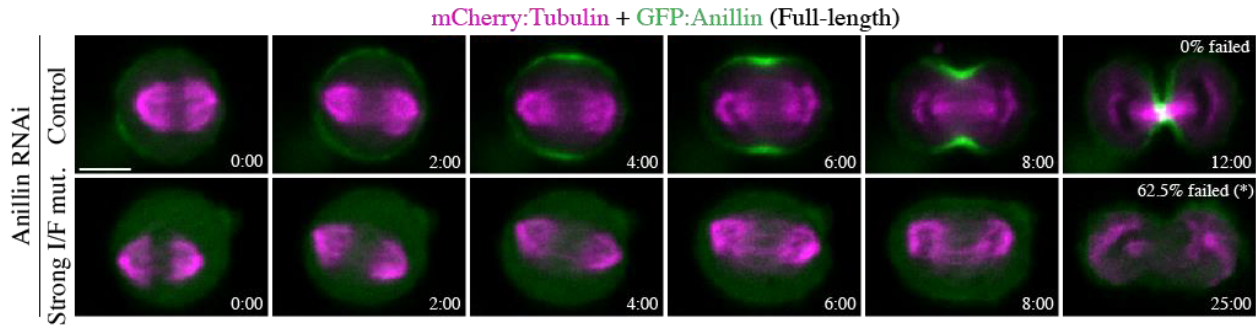
mCherry:Tubulin + GFP:Anillin (Full-length)
Anillin RNAi
Control
Strong I/F mut.
0:00
2:00
4:00
6:00
8:00
12:00
0% failed
0:00
2:00
4:00
6:00
8:00
25:00
62.5% failed (*)

Figure 15. The interface between the RBD and the C2 domain is required for anillin's cortical recruitment and function during cytokinesis. Time-lapse images show HeLa cells treated with anillin RNAi and co-expressing RNAi-resistant GFP-tagged full-length control (n = 15) or strong I/F mutant anillin (n = 16; green) and mCherry:tubulin (magenta). The percentage of cells that failed to complete ingression are indicated. Times are shown in minutes from anaphase onset. The scale bar is 10 μm. I helped perform parts of this experiment with Daniel Beaudet.

A

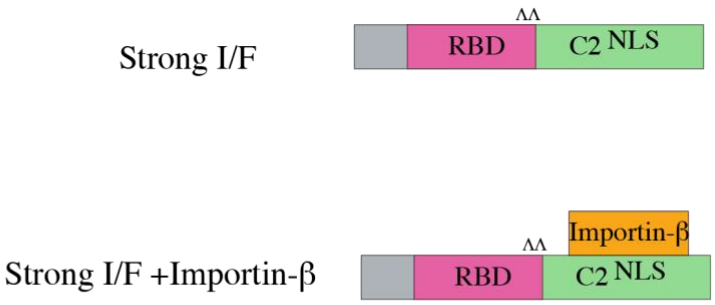

B

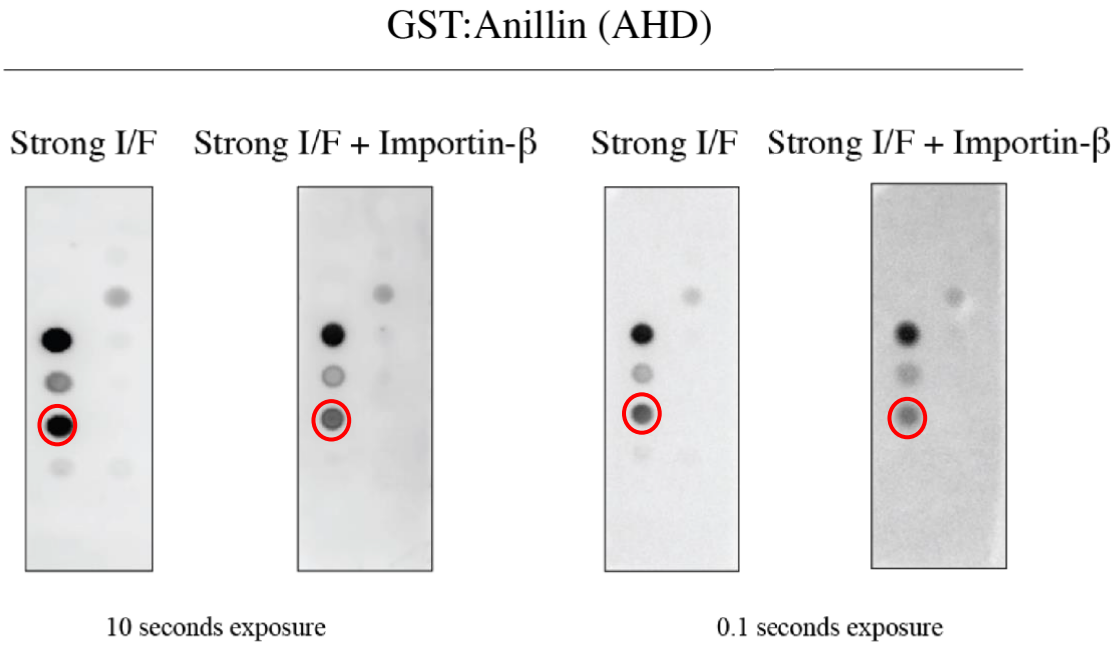

Lysophosphatidic Acid (LPA)	○	○	Sphingosine-1-phosphate (S1P)
Lysophosphocholine (LPC)	○	○	PtdIns(3,4)P2
PtdIns (PI)	○	○	PtdIns(3,5)P2
PtdIns(3)P	○	○	PtdIns(4,5)P2
PtdIns(4)P	○	○	PtdIns(3,4,5)P3
PtdIns(5)P	○	○	Phosphatidic Acid (PA)
Phosphatidylethanolamine (PE)	○	○	Phosphatidylserine (PS)
Phosphatidylcholine (PC)	○	○	Blue Blank

Figure 16. Importin-beta competes with phospholipids for strong I/F mutant binding. A. A cartoon schematic of the open conformation of anillin caused by the strong I/F (indicated by ^^) in the presence and absence of importin-beta (anillin-AHD; RBD (pink) + C2 domain (green)). B. Images of immunoblots show lipid strips after incubation with GST-tagged strong I/F mutant (AHD), and in the presence of importin-beta. Different exposure times (10 seconds, left; 0.1 seconds, right) are shown to highlight the relative changes in phospholipid-binding (PtdIns(5)P is circled in red. Beneath, a schematic shows the position of the different lipids on the strips.

Chapter 5. Discussion

This thesis sheds light on 1) how the requirement for anillin varies among different cell types, and 2) the intramolecular regulation of anillin by importin binding during cytokinesis. The tight spatiotemporal regulation of cytokinesis is accomplished by multiple pathways that work redundantly to avoid cytokinetic errors. While the spindle-dependent pathways are relatively well-studied, spindle-independent pathways are under-explored. Our lab and others found a novel chromatin pathway that utilizes the mitotic Ran-GTP gradient to regulate cytokinesis (Beaudet et al., 2017, 2020; Kiyomitsu & Cheeseman, 2013). This pathway senses chromosomes to properly position the contractile ring and prevent aneuploidy. While Ran-GTP levels are high around chromatin, there is an inverse gradient of importins that are free to bind NLS-containing proteins near the cortex. We found that importin-beta binds to anillin to facilitate its recruitment to the equatorial cortex (Beaudet et al., 2017, 2020). Since the majority of our knowledge of mammalian cell cytokinesis was generated using HeLa cells, it is not clear how the different pathways control cytokinesis in different cell types. Specifically, growing evidence suggests that the mechanisms controlling cytokinesis vary widely between different cell types, and there is a need to study cytokinesis in different contexts (Davies et al., 2018; Herszterg et al., 2014; Ozugergin & Piekny, 2020). Anillin acts as a hub to coordinate multiple pathways and regulators, making it an ideal protein to study cytokinesis mechanisms. In this thesis, we show that anillin has different requirements in different cultured human cells, and develop a tool to precisely measure endogenous anillin levels. We also uncovered the mechanism by which importin binding mediates the cortical recruitment of anillin during cytokinesis.

In Chapter 3, the overall goal of the study is to determine the requirement of anillin in different cell types. We propose that this requirement varies partly with ploidy, as one of the mechanisms that regulates cytokinesis involves chromatin-sensing. As mentioned above, the Ran-GTP gradient is steeper in cells with greater aneuploidy compared to those that are closer to diploid (Hasegawa et al., 2013). Interestingly, anillin has been reported to be overexpressed in different cancer types and is considered a marker of poor clinical prognosis for several cancers including those of the pancreas, lung, breast and liver cancers (*e.g.,* Hall, 2005; Piekny & Maddox, 2010; Wang et al., 2020; Zhang et al., 2018). As described in the introduction, anillin depletion in mouse models of hepatocellular carcinoma prevented tumor progression without disrupting liver function (Zhang et al., 2018). However, it is not clear why anillin is upregulated, and if this expression is

to support cytokinesis or other cellular processes. We hypothesized that as a target for the chromatin pathway, anillin may be upregulated in cells with greater aneuploidy to support their successful cytokinesis and avoid mitotic catastrophe. We investigated the role of anillin during cytokinesis in cells with different types of aneuploidy. Depletion of endogenous anillin showed a correlation between the proportion of cells that failed cytokinesis and the ploidy of the cells (Figure 7). This suggests that anillin may have different thresholds of requirement in cells with higher aneuploidy. However, variability could arise due to differences in RNAi efficiency or genetic differences. Thus, we induced increased aneuploidy in HCT116 cells and found that there was a ~ 3-fold increase in cytokinesis failure (Figure 8). This supports our hypothesis that there is a higher threshold for anillin in cells with higher chromosomal numbers. These results are exciting as they reveal that cancer cells with high aneuploidy could rely more heavily on anillin to avoid mitotic catastrophe, making it ideal to target as an anti-cancer therapy. However, our data relied on western blots and fixed cell immunofluorescence to visualize changes in endogenous anillin, which lack resolution (e.g. population vs. single cell, or temporal) and cannot be used to study the phenotypes leading to cytokinesis failure.

Live imaging provides improved spatiotemporal resolution to analyze cytokinesis phenotypes. Tagging proteins with fluorophores facilitates the optical tracking of protein localization. Although transgenic probes are commonly used to visualize proteins, they are typically over-expressed, and could differ significantly from endogenous proteins in terms of their interactions and localization (Bukhari & Müller, 2019; Mahen et al., 2014). Hence, using gene-editing tools such as CRISPR-Cas9 to tag the endogenous protein is ideal. We used CRISPR-Cas9 to endogenously tag anillin in HCT116 cells with mNeonGreen, a bright and stable fluorescent protein (Shaner et al., 2013; Figure 9). The endogenous tag enabled us to more accurately determine anillin's requirement in these cells with high spatiotemporal resolution (Figure 10). We found that the absolute minimum threshold of anillin required to support cytokinesis was 5% compared to control levels, but 15% of anillin was required to support successful cytokinesis 100% of the time. We were surprised to observe two different cytokinesis phenotypes, early regression and late regression, with no obvious difference in the levels associated with one phenotype vs. the other (Figure 11). Anillin was shown to regulate the contractile ring to midbody transition in Drosophila S2 cells, but a later phenotype has not been described before to our knowledge (Kechad et al., 2012). It would be interesting to determine what role anillin has in midbody stabilization

and/or abscission. This data also suggests that HCT 116 cells have redundant mechanisms that can support cytokinesis when only very little anillin remains. This is quite different compared to what has been reported for anillin requirement in HeLa cells, where the majority of cells fail cytokinesis upon anillin depletion, and these cells presumably have similar levels of anillin remaining (Beaudet et al., 2017; Piekny & Glotzer, 2008; van Oostende Triplet et al., 2014). Our lab recently tagged endogenous anillin with mNeonGreen in HeLa cells and will perform a similar study. We also plan to increase ploidy in the tagged HCT 116 cells to determine how the threshold requirements for anillin. In addition, it would be ideal to visualize the Ran-GTP gradient in these cell lines using an established FRET probe that would provide a direct read out for the correlation between anillin requirement, ploidy and the Ran-GTP and/or importin-gradient (Hasegawa et al., 2013; Kalab & Heald, 2008). These data would support considering anillin as a therapeutic target for cancers that have gained aneuploidy.

In Chapter 4, we explored the intramolecular regulation of anillin by importin-binding. Previously, our lab found that anillin is regulated by importin-beta binding through an NLS that is adjacent to a phospholipid-binding site in the C2 domain (Figure 5). Mutating the NLS resulted in a delayed recruitment and a decrease of breadth of anillin (Beaudet et al., 2017). Since the NLS and phospholipid-binding sites are close to one another, and both rely on basic residues to mediate interactions, I determined that the NLS mutations did not disrupt phospholipid-binding (Figure 12). Thus, the phenotypes we observed with the NLS mutant were indeed due to loss of importin-binding. Surprisingly, we observed a strong preference for binding of the AHD or AHD NLS mutant to PI_3P lipids, although it was previously reported that the lipid-binding site in the C2 domain binds preferentially to $PI_{4,5}P_2$ lipids (Budnar et al., 2019; Sun et al., 2015). The C-terminus of anillin also contains a PH domain, and this domain alone or in combination with the AHD also has been shown to bind preferentially to $PI_{4,5}P_2$ lipids (Frenette et al., 2012; Liu et al., 2012). Therefore, we expected to observe a shift of lipid preference towards $PI_{4,5}P_2$ when performing the *in vitro* assay with the C-terminus recombinant protein. However, the lipid profile was similar, showing a preference towards PI_3P (Figure 12). The main difference between our study is the use of purified proteins vs. proteins from cell lysates. In cells RhoA binds cooperatively to anillin with phospholipids, and may influence the lipid preference of the complex. Therefore, we hypothesize that the presence of other interactors in a cell would affect the conformation of anillin and the lipid preference when compared to an *in vitro* assay.

Our lab previously found that the C2 domain of anillin is autoinhibited by the adjacent RBD domain. We proposed that binding of active RhoA would make the C2 domain accessible for importins to bind (Beaudet et al., 2017, 2020). Mutating residues that lie at the interface between the C2 and RBD domains (strong I/F) had an increase in affinity for importin-binding. In particular, the C-terminus is not nuclear localized due to inhibition via the RBD. However, the C-terminus with the strong I/F mutations was nuclear localized (Figure 13). Furthermore, the strong I/F mutant bound to importin-beta more strongly compared to non-mutant anillin, and regardless of the levels of active RhoA (Figure 14). Introducing the strong I/F mutation into full-length anillin showed that it prevented anillin from being cortically recruited and from functioning during cytokinesis (Figure 15), despite its ability to bind to RhoA (Beaudet et al., 2020). These results suggest that the position of the C2 domain relative to the RBD is important. It seems that feedback between the two domains is crucial for anillin to perform its function during cytokinesis. We hypothesize that although RhoA likely can bind to the RBD in the strong I/F mutant, it binds too tightly to importin to be outcompeted by phospholipids and cannot transition to the membrane where it is required to support cytokinesis.

In light of the proposed hypothesis, we tested if importin-beta binding to the strong I/F can inhibit phospholipid binding. To do this, we compared the lipid profile of the strong I/F mutant in absence and presence of importin-beta. Although preliminary, there seems to be an overall decrease in lipid binding of the strong I/F in presence of importin-beta (Figure 16). This suggests that the interaction between importin-beta and the strong I/F could decrease the affinity of anillin for phospholipids, which could explain why the strong I/F fails to localize or function (Figure 15). This is in line with previous observations, where the overexpression of importins decrease the recruitment of anillin to the cortex, and support a model where importins only facilitate the cortical recruitment of anillin at optimal levels (Beaudet et al., 2017; Silverman-Gavrila et al., 2008). This experiment needs to be replicated to validate our observations. Furthermore, using phospholipid beads could be more reliable vs. the PIP strips and provide more accurate studies of the effect of importin-beta on anillin's phospholipid-binding.

Previous studies proposed the presence of a feedback mechanism between the binding of RhoA and phospholipids to anillin to mediate its function during cytokinesis (Sun et al., 2015; Budnar et al., 2019). Based on our findings, we propose that the importin-binding facilitates the cortical recruitment of anillin by stabilizing an open conformation that favours and 'hands-off' to

phospholipids where it cooperatively binds with RhoA for enrichment at the equatorial cortex (Figure 17). In anaphase, active RhoA increases and binds to the RBD to relieve autoinhibition of the C2 domain. Importin-beta then binds to the C2 domain to stabilize the open conformation and to facilitate interactions between anillin, phospholipids and active RhoA (Figure 17).

This thesis elucidates the variation of anillin's requirements in different human cell lines and provides a mechanistic insight into the coordinated cortical recruitment of anillin by the chromatin pathway and active RhoA. Chapter 3 highlights the need to use better tools to measure the requirement of anillin during cytokinesis. In addition, it reflects the need to diversify the use of different mammalian cells to determine how mechanisms regulating cytokinesis vary among different tissues and contexts. Adapting CRISPR-Cas9 to tag core regulators of cytokinesis can reveal threshold requirements in different cell types. Chapter 4 demonstrates the intramolecular regulation of anillin by importin-beta. It highlights the coordination of importin-beta, RhoA and phospholipid-binding and how this must occur properly for anillin's function during cytokinesis.

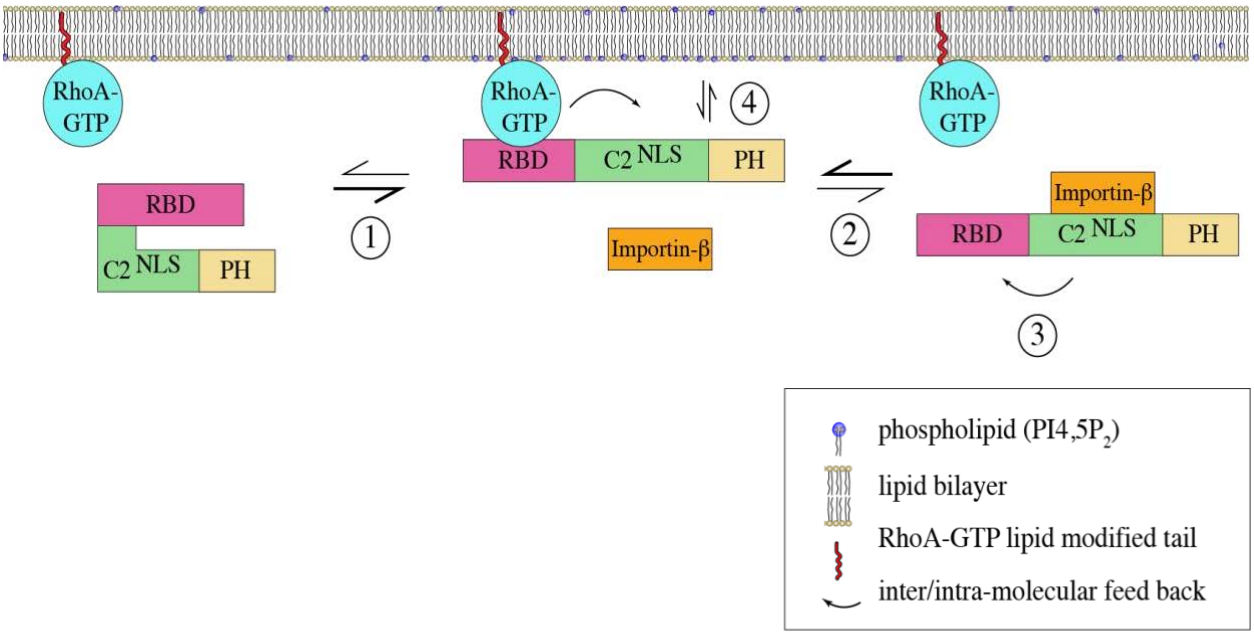
RhoA-GTP
RBD
C2
NLS
PH
1
RhoA-GTP
RBD
C2
NLS
PH
Importin-β
4
2
RhoA-GTP
Importin-β
RBD
C2
NLS
PH
3
phospholipid (PI4,5P2)
lipid bilayer
RhoA-GTP lipid modified tail
inter/intra-molecular feed back

Figure 17. Proposed model of importin-β enhancement to the localization of anillin during cytokinesis. (1) In anaphase onset, RhoA is activated and binds to the RBD (pink) to recruit anillin to the equatorial cortex. Active RhoA (blue) increases the affinity of anillin for importin-β by causing conformational changes between the RBD and C2 domains (green). (2) Near the cortex, importin-β (orange) binds to anillin through the C-terminal NLS, which (3) feeds back to stabilize a conformation that enhances RhoA binding to the RBD by either increasing affinity or reducing dissociation. This figure is adapted from (Beaudet et al., 2020).

Chapter 6. References

Adriaans, I. E., Basant, A., Ponsioen, B., Glotzer, M., & Lens, S. M. A. (2019). PLK1 plays dual roles in centralspindlin regulation during cytokinesis. *Journal of Cell Biology*, *218*(4), 1250–1264. https://doi.org/10.1083/jcb.201805036

Basant, A., & Glotzer, M. (2018). Spatiotemporal Regulation of RhoA during Cytokinesis. *Current Biology*, *28*(9), R570–R580. https://doi.org/10.1016/j.cub.2018.03.045

Basant, A., Lekomtsev, S., Tse, Y. C., Zhang, D., Longhini, K. M., Petronczki, M., & Glotzer, M. (2015). Aurora B Kinase Promotes Cytokinesis by Inducing Centralspindlin Oligomers that Associate with the Plasma Membrane. *Developmental Cell*, *33*(2), 204–215. https://doi.org/10.1016/j.devcel.2015.03.015

Beaudet, D., Akhshi, T., Phillipp, J., Law, C., & Piekny, A. (2017). Active Ran regulates anillin function during cytokinesis. *Molecular Biology of the Cell*, *28*(24), 3517–3531. https://doi.org/10.1091/mbc.e17-04-0253

Beaudet, D., Pham, N., Skaik, N., & Piekny, A. (2020). Importin binding mediates the intramolecular regulation of anillin during cytokinesis. *Molecular Biology of the Cell*, *31*(11), 1124–1139. https://doi.org/10.1091/mbc.E20-01-0006

Budnar, S., Husain, K. B., Gomez, G. A., Naghibosadat, M., Varma, A., Verma, S., Hamilton, N. A., Morris, R. G., & Yap, A. S. (2019). Anillin Promotes Cell Contractility by Cyclic Resetting of RhoA Residence Kinetics. *Developmental Cell*, *49*(6), 894-906.e12. https://doi.org/10.1016/j.devcel.2019.04.031

Bukhari, H., & Müller, T. (2019). Endogenous Fluorescence Tagging by CRISPR. *Trends in Cell Biology*, *29*(11), 912–928. https://doi.org/10.1016/j.tcb.2019.08.004

Canman, J. C., Lewellyn, L., Laband, K., Smerdon, S. J., Desai, A., Bowerman, B., & Oegema, K. (2008). Inhibition of Rac by the GAP Activity of Centralspindlin Is Essential for Cytokinesis. *Science*, *322*(5907), 1543–1546. https://doi.org/10.1126/science.1163086

Chen, A., Akhshi, T. K., Lavoie, B. D., & Wilde, A. (2015). Importin β2 Mediates the Spatio-temporal Regulation of Anillin through a Noncanonical Nuclear Localization Signal. *Journal of Biological Chemistry*, *290*(21), 13500–13509. https://doi.org/10.1074/jbc.M115.649160

Clarke, P. R., & Zhang, C. (2008). Spatial and temporal coordination of mitosis by Ran GTPase. *Nature Reviews Molecular Cell Biology*, *9*(6), 464–477. https://doi.org/10.1038/nrm2410

Davies, T., Kim, H. X., Romano Spica, N., Lesea-Pringle, B. J., Dumont, J., Shirasu-Hiza, M., & Canman, J. C. (2018). Cell-intrinsic and -extrinsic mechanisms promote cell-type-specific cytokinetic diversity. *ELife*, *7*, e36204. https://doi.org/10.7554/eLife.36204

D'Avino, P. P., Giansanti, M. G., & Petronczki, M. (2015). Cytokinesis in Animal Cells. *Cold Spring Harbor Perspectives in Biology*, *7*(4), a015834. https://doi.org/10.1101/cshperspect.a015834

Deng, M., Suraneni, P., Schultz, R. M., & Li, R. (2007). The Ran GTPase Mediates Chromatin Signaling to Control Cortical Polarity during Polar Body Extrusion in Mouse Oocytes. *Developmental Cell*, *12*(2), 301–308. https://doi.org/10.1016/j.devcel.2006.11.008

Douglas, M. E., Davies, T., Joseph, N., & Mishima, M. (2010). Aurora B and 14-3-3 Coordinately Regulate Clustering of Centralspindlin during Cytokinesis. *Current Biology*, *20*(10), 927–933. https://doi.org/10.1016/j.cub.2010.03.055

El Amine, N., Kechad, A., Jananji, S., & Hickson, G. R. X. (2013). Opposing actions of septins and Sticky on Anillin promote the transition from contractile to midbody ring. *The Journal of Cell Biology*, *203*(3), 487–504. https://doi.org/10.1083/jcb.201305053

Fededa, J. P., & Gerlich, D. W. (2012). Molecular control of animal cell cytokinesis. *Nature Cell Biology*, *14*(5), 440–447. https://doi.org/10.1038/ncb2482

Field, C. M., & Alberts, B. M. (1995). Anillin, a contractile ring protein that cycles from the nucleus to the cell cortex. *The Journal of Cell Biology*, *131*(1), 165–178. https://doi.org/10.1083/jcb.131.1.165

Forbes, D. J., Travesa, A., Nord, M. S., & Bernis, C. (2015). Nuclear transport factors: Global regulation of mitosis. *Current Opinion in Cell Biology*, *35*, 78–90. https://doi.org/10.1016/j.ceb.2015.04.012

Frenette, P., Haines, E., Loloyan, M., Kinal, M., Pakarian, P., & Piekny, A. (2012). An Anillin-Ect2 Complex Stabilizes Central Spindle Microtubules at the Cortex during Cytokinesis. *PLoS ONE*, *7*(4), e34888. https://doi.org/10.1371/journal.pone.0034888

Gai, M., Camera, P., Dema, A., Bianchi, F., Berto, G., Scarpa, E., Germena, G., & Di Cunto, F. (2011). Citron kinase controls abscission through RhoA and anillin. *Molecular Biology of the Cell*, *22*(20), 3768–3778. https://doi.org/10.1091/mbc.e10-12-0952

Glotzer, M. (2009). The 3Ms of central spindle assembly: Microtubules, motors and MAPs. *Nature Reviews Molecular Cell Biology*, *10*(1), 9–20. https://doi.org/10.1038/nrm2609

Glotzer, M. (2017). Cytokinesis in Metazoa and Fungi. *Cold Spring Harbor Perspectives in Biology*, *9*(10), a022343. https://doi.org/10.1101/cshperspect.a022343

Green, R. A., Paluch, E., & Oegema, K. (2012). Cytokinesis in Animal Cells. *Annual Review of Cell and Developmental Biology*, *28*(1), 29–58. https://doi.org/10.1146/annurev-cellbio-101011-155718

Guse, A., Mishima, M., & Glotzer, M. (2005). Phosphorylation of ZEN-4/MKLP1 by Aurora B Regulates Completion of Cytokinesis. *Current Biology*, *15*(8), 778–786. https://doi.org/10.1016/j.cub.2005.03.041

Haglund, K., Nezis, I. P., Lemus, D., Grabbe, C., Wesche, J., Liestøl, K., Dikic, I., Palmer, R., & Stenmark, H. (2010). Cindr Interacts with Anillin to Control Cytokinesis in Drosophila melanogaster. *Current Biology*, *20*(10), 944–950. https://doi.org/10.1016/j.cub.2010.03.068

Hall, P. A. (2005). The Septin-Binding Protein Anillin Is Overexpressed in Diverse Human Tumors. *Clinical Cancer Research*, *11*(19), 6780–6786. https://doi.org/10.1158/1078-0432.CCR-05-0997

Hara, T., Abe, M., Inoue, H., Yu, L.-R., Veenstra, T. D., Kang, Y. H., Lee, K. S., & Miki, T. (2006). Cytokinesis regulator ECT2 changes its conformation through phosphorylation at Thr-341 in G2/M phase. *Oncogene*, *25*(4), 566–578. https://doi.org/10.1038/sj.onc.1209078

Hasegawa, K., Ryu, S. J., & Kaláb, P. (2013). Chromosomal gain promotes formation of a steep RanGTP gradient that drives mitosis in aneuploid cells. *The Journal of Cell Biology*, *200*(2), 151–161. https://doi.org/10.1083/jcb.201206142

Herszterg, S., Pinheiro, D., & Bellaïche, Y. (2014). A multicellular view of cytokinesis in epithelial tissue. *Trends in Cell Biology*, *24*(5), 285–293. https://doi.org/10.1016/j.tcb.2013.11.009

Hickson, G. R. X., & O'Farrell, P. H. (2008). Rho-dependent control of anillin behavior during cytokinesis. *Journal of Cell Biology*, *180*(2), 285–294. https://doi.org/10.1083/jcb.200709005

Kalab, P., & Heald, R. (2008). The RanGTP gradient—A GPS for the mitotic spindle. *Journal of Cell Science*, *121*(10), 1577–1586. https://doi.org/10.1242/jcs.005959

Kaláb, P., Pralle, A., Isacoff, E. Y., Heald, R., & Weis, K. (2006). Analysis of a RanGTP-regulated gradient in mitotic somatic cells. *Nature*, *440*(7084), 697–701. https://doi.org/10.1038/nature04589

Kamijo, K., Ohara, N., Abe, M., Uchimura, T., Hosoya, H., Lee, J.-S., & Miki, T. (2006). Dissecting the Role of Rho-mediated Signaling in Contractile Ring Formation□D □V. *Molecular Biology of the Cell*, *17*, 13.

Kechad, A., Jananji, S., Ruella, Y., & Hickson, G. R. X. (2012). Anillin Acts as a Bifunctional Linker Coordinating Midbody Ring Biogenesis during Cytokinesis. *Current Biology*, *22*(3), 197–203. https://doi.org/10.1016/j.cub.2011.11.062

Kiyomitsu, T., & Cheeseman, I. M. (2013). Cortical Dynein and Asymmetric Membrane Elongation Coordinately Position the Spindle in Anaphase. *Cell*, *154*(2), 391–402. https://doi.org/10.1016/j.cell.2013.06.010

Kotýnková, K., Su, K.-C., West, S. C., & Petronczki, M. (2016). Plasma Membrane Association but Not Midzone Recruitment of RhoGEF ECT2 Is Essential for Cytokinesis. *Cell Reports*, *17*(10), 2672–2686. https://doi.org/10.1016/j.celrep.2016.11.029

Lekomtsev, S., Su, K.-C., Pye, V. E., Blight, K., Sundaramoorthy, S., Takaki, T., Collinson, L. M., Cherepanov, P., Divecha, N., & Petronczki, M. (2012). Centralspindlin links the mitotic spindle to the plasma membrane during cytokinesis. *Nature*, *492*(7428), 276–279. https://doi.org/10.1038/nature11773

Liu, J., Fairn, G. D., Ceccarelli, D. F., Sicheri, F., & Wilde, A. (2012). Cleavage Furrow Organization Requires PIP2-Mediated Recruitment of Anillin. *Current Biology*, *22*(1), 64–69. https://doi.org/10.1016/j.cub.2011.11.040

Lopez-Sánchez, L. M., Jimenez, C., Valverde, A., Hernandez, V., Peñarando, J., Martinez, A., Lopez-Pedrera, C., Muñoz-Castañeda, J. R., De la Haba-Rodríguez, J. R., Aranda, E., & Rodriguez-Ariza, A. (2014). CoCl2, a Mimic of Hypoxia, Induces Formation of Polyploid Giant Cells with Stem Characteristics in Colon Cancer. *PLoS ONE*, *9*(6), e99143. https://doi.org/10.1371/journal.pone.0099143

Maddox, A. S. (2005). Distinct roles for two C. elegans anillins in the gonad and early embryo. *Development*, *132*(12), 2837–2848. https://doi.org/10.1242/dev.01828

Maddox, Amy Shaub, Lewellyn, L., Desai, A., & Oegema, K. (2007). Anillin and the Septins Promote Asymmetric Ingression of the Cytokinetic Furrow. *Developmental Cell*, *12*(5), 827–835. https://doi.org/10.1016/j.devcel.2007.02.018

Mahen, R., Koch, B., Wachsmuth, M., Politi, A. Z., Perez-Gonzalez, A., Mergenthaler, J., Cai, Y., & Ellenberg, J. (2014). Comparative assessment of fluorescent transgene methods for quantitative imaging in human cells. *Molecular Biology of the Cell*, *25*(22), 3610–3618. https://doi.org/10.1091/mbc.e14-06-1091

Mangal, S., Sacher, J., Kim, T., Osório, D. S., Motegi, F., Carvalho, A. X., Oegema, K., & Zanin, E. (2018). TPXL-1 activates Aurora A to clear contractile ring components from the polar cortex during cytokinesis. *Journal of Cell Biology*, *217*(3), 837–848. https://doi.org/10.1083/jcb.201706021

Mishima, M., Kaitna, S., & Glotzer, M. (2002). Central Spindle Assembly and Cytokinesis Require a Kinesin-like Protein/RhoGAP Complex with Microtubule Bundling Activity. *Developmental Cell*, *2*(1), 41–54. https://doi.org/10.1016/S1534-5807(01)00110-1

Mishima, M., Pavicic, V., Grüneberg, U., Nigg, E. A., & Glotzer, M. (2004). Cell cycle regulation of central spindle assembly. *Nature*, *430*(7002), 908–913. https://doi.org/10.1038/nature02767

Mollinari, C., Kleman, J.-P., Saoudi, Y., Jablonski, S. A., Perard, J., Yen, T. J., & Margolis, R. L. (2005). Ablation of PRC1 by Small Interfering RNA Demonstrates that Cytokinetic Abscission Requires a Central Spindle Bundle in Mammalian Cells, whereas Completion of Furrowing Does Not□V. *Molecular Biology of the Cell*, *16*, 13.

Niiya, F., Tatsumoto, T., Lee, K. S., & Miki, T. (2006). Phosphorylation of the cytokinesis regulator ECT2 at G2/M phase stimulates association of the mitotic kinase Plk1 and accumulation of GTP-bound RhoA. *Oncogene*, *25*(6), 827–837. https://doi.org/10.1038/sj.onc.1209124

Nishimura, Y. (2006). Centralspindlin regulates ECT2 and RhoA accumulation at the equatorial cortex during cytokinesis. *Journal of Cell Science*, *119*(1), 104–114. https://doi.org/10.1242/jcs.02737

Oegema, K., Savoian, M. S., Mitchison, T. J., & Field, C. M. (2000). Functional Analysis of a Human Homologue of the Drosophila Actin Binding Protein Anillin Suggests a Role in

Cytokinesis. *Journal of Cell Biology*, *150*(3), 539–552. https://doi.org/10.1083/jcb.150.3.539

Ozugergin, I., & Piekny, A. (2020). Complementary functions for the Ran gradient during division. *Small GTPases*, 1–11. https://doi.org/10.1080/21541248.2020.1725371

Pavicic-Kaltenbrunner, V., Mishima, M., & Glotzer, M. (2007). Cooperative Assembly of CYK-4/MgcRacGAP and ZEN-4/MKLP1 to Form the Centralspindlin Complex□D □V. *Molecular Biology of the Cell*, *18*, 12.

Petronczki, M., Glotzer, M., Kraut, N., & Peters, J.-M. (2007). Polo-like Kinase 1 Triggers the Initiation of Cytokinesis in Human Cells by Promoting Recruitment of the RhoGEF Ect2 to the Central Spindle. *Developmental Cell*, *12*(5), 713–725. https://doi.org/10.1016/j.devcel.2007.03.013

Piekny, A. J., & Glotzer, M. (2008). Anillin Is a Scaffold Protein That Links RhoA, Actin, and Myosin during Cytokinesis. *Current Biology*, *18*(1), 30–36. https://doi.org/10.1016/j.cub.2007.11.068

Piekny, A. J., & Maddox, A. S. (2010). The myriad roles of Anillin during cytokinesis. *Seminars in Cell & Developmental Biology*, *21*(9), 881–891. https://doi.org/10.1016/j.semcdb.2010.08.002

Piekny, A., Werner, M., & Glotzer, M. (2005). Cytokinesis: Welcome to the Rho zone. *Trends in Cell Biology*, *15*(12), 651–658. https://doi.org/10.1016/j.tcb.2005.10.006

Pollard, T. D. (2017). Nine unanswered questions about cytokinesis. *Journal of Cell Biology*, *216*(10), 3007–3016. https://doi.org/10.1083/jcb.201612068

Pollard, T. D., & O'Shaughnessy, B. (2019). Molecular Mechanism of Cytokinesis. *Annual Review of Biochemistry*, *88*(1), 661–689. https://doi.org/10.1146/annurev-biochem-062917-012530

Reyes, C. C., Jin, M., Breznau, E. B., Espino, R., Delgado-Gonzalo, R., Goryachev, A. B., & Miller, A. L. (2014). Anillin Regulates Cell-Cell Junction Integrity by Organizing Junctional Accumulation of Rho-GTP and Actomyosin. *Current Biology*, *24*(11), 1263–1270. https://doi.org/10.1016/j.cub.2014.04.021

Rodrigues, N. T. L., Lekomtsev, S., Jananji, S., Kriston-Vizi, J., Hickson, G. R. X., & Baum, B. (2015). Kinetochore-localized PP1–Sds22 couples chromosome segregation to polar relaxation. *Nature*, *524*(7566), 489–492. https://doi.org/10.1038/nature14496

Shaner, N. C., Lambert, G. G., Chammas, A., Ni, Y., Cranfill, P. J., Baird, M. A., Sell, B. R., Allen, J. R., Day, R. N., Israelsson, M., Davidson, M. W., & Wang, J. (2013). A bright monomeric green fluorescent protein derived from Branchiostoma lanceolatum. *Nature Methods*, *10*(5), 407–409. https://doi.org/10.1038/nmeth.2413

Silverman-Gavrila, R. V., Hales, K. G., & Wilde, A. (2008). Anillin-mediated Targeting of Peanut to Pseudocleavage Furrows Is Regulated by the GTPase Ran. *Molecular Biology of the Cell*, *19*(9), 3735–3744. https://doi.org/10.1091/mbc.e08-01-0049

Soniat, M., & Chook, Y. M. (2015). Nuclear localization signals for four distinct karyopherin-β nuclear import systems. *Biochemical Journal*, *468*(3), 353–362. https://doi.org/10.1042/BJ20150368

Storchova, Z., & Pellman, D. (2004). From polyploidy to aneuploidy, genome instability and cancer. *Nature Reviews Molecular Cell Biology*, *5*(1), 45–54. https://doi.org/10.1038/nrm1276

Straight, A. F., Field, C. M., & Mitchison, T. J. (2005). Anillin Binds Nonmuscle Myosin II and Regulates the Contractile Ring□D □V. *Molecular Biology of the Cell*, *16*, 9.

Sun, L., Guan, R., Lee, I.-J., Liu, Y., Chen, M., Wang, J., Wu, J.-Q., & Chen, Z. (2015). Mechanistic Insights into the Anchorage of the Contractile Ring by Anillin and Mid1. *Developmental Cell*, *33*(4), 413–426. https://doi.org/10.1016/j.devcel.2015.03.003

Tse, Y. C., Piekny, A., & Glotzer, M. (2011). Anillin promotes astral microtubule-directed cortical myosin polarization. *Molecular Biology of the Cell*, *22*(17), 3165–3175. https://doi.org/10.1091/mbc.e11-05-0399

van Oostende Triplet, C., Jaramillo Garcia, M., Haji Bik, H., Beaudet, D., & Piekny, A. (2014). Anillin interacts with microtubules and is part of the astral pathway that defines cortical domains. *Journal of Cell Science*, *127*(17), 3699–3710. https://doi.org/10.1242/jcs.147504

Wang, D., Naydenov, N. G., Dozmorov, M. G., Koblinski, J. E., & Ivanov, A. I. (2020). Anillin regulates breast cancer cell migration, growth, and metastasis by non-canonical mechanisms involving control of cell stemness and differentiation. *Breast Cancer Research*, *22*(1), 3. https://doi.org/10.1186/s13058-019-1241-x

Watanabe, S., Okawa, K., Miki, T., Sakamoto, S., Morinaga, T., Segawa, K., Arakawa, T., Kinoshita, M., Ishizaki, T., & Narumiya, S. (2010). Rho and Anillin-dependent Control of

mDia2 Localization and Function in Cytokinesis. *Molecular Biology of the Cell*, *21*(18), 3193–3204. https://doi.org/10.1091/mbc.e10-04-0324

Werner, M., Munro, E., & Glotzer, M. (2007). Astral Signals Spatially Bias Cortical Myosin Recruitment to Break Symmetry and Promote Cytokinesis. *Current Biology*, *17*(15), 1286–1297. https://doi.org/10.1016/j.cub.2007.06.070

Wernike, D., Chen, Y., Mastronardi, K., Makil, N., & Piekny, A. (2016). Mechanical forces drive neuroblast morphogenesis and are required for epidermal closure. *Developmental Biology*, *412*(2), 261–277. https://doi.org/10.1016/j.ydbio.2016.02.023

Wolfe, B. A., Takaki, T., Petronczki, M., & Glotzer, M. (2009). Polo-Like Kinase 1 Directs Assembly of the HsCyk-4 RhoGAP/Ect2 RhoGEF Complex to Initiate Cleavage Furrow Formation. *PLoS Biology*, *7*(5), e1000110. https://doi.org/10.1371/journal.pbio.1000110

Xu, L., & Massagué, J. (2004). Nucleocytoplasmic shuttling of signal transducers. *Nature Reviews Molecular Cell Biology*, *5*(3), 209–219. https://doi.org/10.1038/nrm1331

Yüce, Ö., Piekny, A., & Glotzer, M. (2005). An ECT2–centralspindlin complex regulates the localization and function of RhoA. *Journal of Cell Biology*, *170*(4), 571–582. https://doi.org/10.1083/jcb.200501097

Zanin, E., Desai, A., Poser, I., Toyoda, Y., Andree, C., Moebius, C., Bickle, M., Conradt, B., Piekny, A., & Oegema, K. (2013). A Conserved RhoGAP Limits M Phase Contractility and Coordinates with Microtubule Asters to Confine RhoA during Cytokinesis. *Developmental Cell*, *26*(5), 496–510. https://doi.org/10.1016/j.devcel.2013.08.005

Zhang, S., Nguyen, L. H., Zhou, K., Tu, H.-C., Sehgal, A., Nassour, I., Li, L., Gopal, P., Goodman, J., Singal, A. G., Yopp, A., Zhang, Y., Siegwart, D. J., & Zhu, H. (2018). Knockdown of Anillin Actin Binding Protein Blocks Cytokinesis in Hepatocytes and Reduces Liver Tumor Development in Mice Without Affecting Regeneration. *Gastroenterology*, *154*(5), 1421–1434. https://doi.org/10.1053/j.gastro.2017.12.013

Zhao, W. -m., & Fang, G. (2005). MgcRacGAP controls the assembly of the contractile ring and the initiation of cytokinesis. *Proceedings of the National Academy of Sciences*, *102*(37), 13158–13163. https://doi.org/10.1073/pnas.0504145102